An Analytic Approximation to the Bayesian Detection Statistic for Continuous Gravitational Waves

John J. Bero

Center for Computational Relativity and Gravitation and School of Physics and Astronomy, Rochester Institute of Technology, 84 Lomb Memorial Drive, Rochester, NY 14623, United States of America

John T. Whelan

E-mail: john.whelan@astro.rit.edu
Center for Computational Relativity and Gravitation and School of Mathematical Sciences, Rochester Institute of Technology, 85 Lomb Memorial Drive, Rochester, NY 14623, United States of America

Abstract. We consider the Bayesian detection statistic for a targeted search for continuous gravitational waves, known as the $\mathcal{B}$-statistic. This is a Bayes factor between signal and noise hypotheses, produced by marginalizing over the four amplitude parameters of the signal. We show that by Taylor-expanding to first order in certain averaged combinations of antenna patterns (elements of the parameter space metric), the marginalization integral can be performed analytically, producing a closed-form approximation in terms of confluent hypergeometric functions. We demonstrate using Monte Carlo simulations that this approximation is as powerful as the full $\mathcal{B}$-statistic, and outperforms the traditional maximum-likelihood $\mathcal{F}$-statistic, for several observing scenarios which involve an average over sidereal times. We also show that the approximation does not perform well for a near-instantaneous observation, so the approximation is suited to continuous wave observations rather than transient modelled signals such as compact binary inspiral.

1. Introduction

The signal from a non-precessing source of gravitational waves (GWs) such as a rotating neutron star or slowly-evolving binary system, can be described by phase-evolution parameters, which determine the shape of the signal, and amplitude parameters. In the case where the phase-evolution parameters are assumed to be known, the likelihood ratio between models with and without signal is a function of the four amplitude parameters. Jaranowski, Królak and Schutz [1] constructed a maximum-likelihood statistic (known as the $\mathcal{F}$-statistic), which is the basis of many existing searches for continuous GWs. Prix and Krishnan [2] proposed a Bayesian alternative (the $\mathcal{B}$-statistic) which instead marginalized the likelihood ratio over these parameters, assuming a geometrically-inspired prior distribution. Exact evaluation of the $\mathcal{B}$-statistic requires integration over the four-dimensional amplitude parameter space; Whelan et al [3] showed that two of the integrals can be done analytically, but a two-dimensional numerical integration remains. They also showed that the marginalization integrals can be done exactly if the parameter-space metric (determined by averaged combinations of antenna patterns) has a block-diagonal form. In this paper, we generalize this result to produce an analytical approximation to the $\mathcal{B}$-statistic by Taylor expanding to first order in the off-diagonal metric elements.

This paper is laid out as follows: in section 2 we give a brief overview of the background information and formalism related to this topic, including a discussion of GW signal analysis and a description of the two detection statistics which already exist. Section 3 contains the derivation of our approximation and in section 4 we test the power of the approximation as a detection statistic. Section 5 concludes with a summary of the results and their practical implications.

2. Formalism

2.1. Signal Parameters

We follow the conventions and notation of [3], where more details can be found. We summarize the relevant expressions here. For a GW signal coming from a sky position specified by right ascension α and declination δ, we can define a propagation unit vector $\vec{k}$ pointing from the source to the solar-system barycenter (SSB). The tensor GW can then be resolved in a basis of traceless tensors transverse to $\vec{k}$ as

$$\overleftrightarrow{h}(\tau) = h_+(\tau)\,\overleftrightarrow{e}_+ + h_\times(\tau)\,\overleftrightarrow{e}_\times \ . \tag{2.1}$$

For a nearly periodic signal, as from a rotating neutron star (NS), the polarization components are

$$h_+(\tau) \equiv \frac{h_0}{2}(1+\chi^2)\cos[\phi(\tau)+\phi_0] \qquad \text{and} \qquad h_\times(\tau) \equiv h_0\chi\sin[\phi(\tau)+\phi_0] \ , \tag{2.2}$$

where $\chi = \cos\iota$ is the cosine of angle between the line of sight and the neutron star's rotation axis, and

$$h_0 = \frac{4G}{c^4}\frac{|I_{xx} - I_{yy}|\,\Omega^2}{d} \tag{2.3}$$

is the amplitude in terms of the equatorial quadrupole moments $\{I_{xx}, I_{yy}\}$, the rotation frequency Ω, and the distance d to the source. The preferred polarization basis tensors are given by

$$\overleftrightarrow{e}_+ = \overleftrightarrow{\varepsilon}_+ \cos 2\psi + \overleftrightarrow{\varepsilon}_\times \sin 2\psi \qquad \text{and} \qquad \overleftrightarrow{e}_\times = -\overleftrightarrow{\varepsilon}_+ \sin 2\psi + \overleftrightarrow{\varepsilon}_\times \cos 2\psi \; . \tag{2.4}$$

where $\overleftrightarrow{\varepsilon}_+ = \vec{\imath}\otimes\vec{\imath} - \vec{\jmath}\otimes\vec{\jmath}$ and $\overleftrightarrow{\varepsilon}_\times = \vec{\imath}\otimes\vec{\jmath} + \vec{\jmath}\otimes\vec{\imath}$ are the fiducial basis tensors defined using unit vectors orthogonal to $\vec{k}$, with $\vec{\imath}$ pointing "West on the sky" in the direction of decreasing right ascension α, and $\vec{\jmath}$ pointing "North on the sky" in the direction of increasing declination δ. The polarization angle ψ measures the angle counter-clockwise on the sky from $\vec{\imath}$ to the NS's equatorial plane.

The phase evolution $\phi(\tau)$ in terms of the arrival time τ at the SSB can be written in terms of NS rotation or spindown parameters, e.g.,

$$\phi(\tau) = 2\pi\left(f_0\tau + f_1\frac{\tau^2}{2} + \cdots\right) \; , \tag{2.5}$$

although it may be more complicated, e.g., for NSs in binary systems.

The strain, h, measured by an interferometric GW detector whose arms are parallel to the unit vectors $\vec{p}_1$ and $\vec{p}_2$ is given by

$$h = \overleftrightarrow{h} : \overleftrightarrow{d} \tag{2.6}$$

where‡

$$\overleftrightarrow{d} = \frac{\vec{p}_1\otimes\vec{p}_1 - \vec{p}_2\otimes\vec{p}_2}{2} \tag{2.7}$$

is the detector tensor and : signifies the double dot product, defined by $(\vec{a}\otimes\vec{b}) : (\vec{c}\otimes\vec{d}) = (\vec{a}\cdot\vec{d})(\vec{b}\cdot\vec{c})$. The GW strain can also be expressed as

$$h = h_+F_+ + h_\times F_\times \; , \tag{2.8}$$

where F_+ and $F_\times$ are the detector antenna pattern functions which depend on the 3 angles defining the source sky position and polarization basis relative to your detector, which in our case would be the right ascension α, the declination δ and the polarization angle ψ. If we separate out their dependence on ψ, then the pattern functions have the form

$$F_+(\alpha,\delta,\psi) = \; a(\alpha,\delta)\cos 2\psi + b(\alpha,\delta)\sin 2\psi \tag{2.9a}$$

$$F_\times(\alpha,\delta,\psi) = -a(\alpha,\delta)\sin 2\psi + b(\alpha,\delta)\cos 2\psi \; , \tag{2.9b}$$

‡ We limit attention in this section to the long-wavelength limit, where the detectors are assumed to be small compared to the gravitational wavelength c/f_0, which is appropriate to most observations with ground-based interferometric detectors. At higher frequencies, the detector tensor $\overleftrightarrow{d}(f)$ is frequency-dependent and complex. See e.g.,[3] for more details.

where a and b are amplitude modulation coefficients defined in terms of the detector tensor $\overset{\leftrightarrow}{d}$ as

$$a \equiv \overset{\leftrightarrow}{\varepsilon}_{+} : \overset{\leftrightarrow}{d} \,, \tag{2.10a}$$

$$b \equiv \overset{\leftrightarrow}{\varepsilon}_{\times} : \overset{\leftrightarrow}{d} \,. \tag{2.10b}$$

These coefficients are defined with respect to the reference polarization basis and depend both on the sky position of the GW source and the sidereal time at which the measurement is taking place.

It is useful to divide the signal parameters into *amplitude parameters*§ $\{h_0, \chi, \psi, \phi_0\}$ and *phase-evolution parameters* such as the sky position $\{\alpha, \delta\}$, and any parameters describing $\phi(\tau)$. The dependence of the signal on the amplitude parameters can be written simply as[1, 3]

$$\overset{\leftrightarrow}{h}(\tau; \mathcal{A}, \lambda) = \mathcal{A}^{\check{\mu}} \overset{\leftrightarrow}{h}_{\check{\mu}}(\tau; \lambda) \,, \tag{2.11}$$

where the Einstein summation convention implies the sum $\sum_{\mu=1}^{4}$ over repeated indices. The amplitudes $\{\mathcal{A}^{\check{\mu}}\}$ are defined by‖

$$\mathcal{A}^{\check{1}} = A_{\mathrm{R}} \cos\phi_{\mathrm{R}} \qquad \text{and} \qquad \mathcal{A}^{\check{2}} = A_{\mathrm{R}} \sin\phi_{\mathrm{R}} \,; \tag{2.12a}$$

$$\mathcal{A}^{\check{3}} = A_{\mathrm{L}} \cos\phi_{\mathrm{L}} \qquad \text{and} \qquad \mathcal{A}^{\check{4}} = A_{\mathrm{L}} \sin\phi_{\mathrm{L}} \,, \tag{2.12b}$$

where

$$A_{\mathrm{R}} = h_0 \left(\frac{1+\chi}{2}\right)^2 \quad \text{and} \quad \phi_{\mathrm{R}} = \phi_0 + 2\psi \,; \tag{2.13a}$$

$$A_{\mathrm{L}} = h_0 \left(\frac{1-\chi}{2}\right)^2 \quad \text{and} \quad \phi_{\mathrm{L}} = \phi_0 - 2\psi \tag{2.13b}$$

are the amplitudes and phases of the right- and left-circularly-polarized components of the signal, respectively.

2.2. Likelihood Function and Detection Statistics

If we denote the data recorded in the GW detector(s) as x, and assume those data to consist of the signal $\mathcal{A}^{\check{\mu}} h_{\check{\mu}}$ plus Gaussian noise, the sampling distribution for the data will be

$$\mathrm{pdf}(x|\mathcal{A}) \propto \exp\left(-\frac{1}{2}\left(x - \mathcal{A}^{\check{\mu}} h_{\check{\mu}} | x - \mathcal{A}^{\check{\mu}} h_{\check{\mu}}\right)\right) \tag{2.14}$$

The log-likelihood ratio will thus be

$$\Lambda(\{\mathcal{A}^{\check{\mu}}\}; x) = \ln \frac{\mathrm{pdf}(x|\mathcal{A})}{\mathrm{pdf}(x|0)} = \mathcal{A}^{\check{\mu}} x_{\check{\mu}} - \frac{1}{2} \mathcal{A}^{\check{\mu}} \mathcal{M}_{\check{\mu}\check{\nu}} \mathcal{A}^{\check{\nu}} \tag{2.15}$$

§ Note that ϕ_0 is considered an amplitude parameter because it does not affect the *time evolution* of the phase $\phi(\tau)$ appearing in (2.2), which could be rewritten in terms of amplitudes $h_c = h_0 \cos\phi_0$ and $h_s = h_0 \sin\phi_0$.

‖ Our coordinates $\{\mathcal{A}^{\check{\mu}}\}$, introduced in [3], are related to the more familiar Jaranowski-Królak-Schutz (JKS) coordinates $\{\mathcal{A}^{\mu}\}$ of [1] by $\mathcal{A}^1 = \mathcal{A}^{\check{1}} + \mathcal{A}^{\check{3}}$, $\mathcal{A}^2 = \mathcal{A}^{\check{2}} - \mathcal{A}^{\check{4}}$, $\mathcal{A}^3 = -\mathcal{A}^{\check{2}} - \mathcal{A}^{\check{4}}$, $\mathcal{A}^4 = \mathcal{A}^{\check{1}} - \mathcal{A}^{\check{3}}$.

where $x_{\check{\mu}} \equiv (x|h_{\check{\mu}})$ is the scalar product (see Appendix A) of the data with the template waveform, and

$$\{\mathcal{M}_{\check{\mu}\check{\nu}}\} \equiv \{(h_{\check{\mu}}|h_{\check{\nu}})\} = \begin{pmatrix} I & 0 & L & -K \\ 0 & I & K & L \\ L & K & J & 0 \\ -K & L & 0 & J \end{pmatrix} \tag{2.16}$$

forms a metric on parameter space.

If we define $\{\mathcal{M}^{\check{\mu}\check{\nu}}\}$ as the matrix inverse of $\{\mathcal{M}_{\check{\mu}\check{\nu}}\}$, we can write the maximum-likelihood values of the amplitude parameters $\{\mathcal{A}^{\check{\mu}}\}$ as

$$\widehat{\mathcal{A}}^{\check{\mu}}(x) = \mathcal{M}^{\check{\mu}\check{\nu}} x_{\check{\nu}} \ , \tag{2.17}$$

Since the maximum-likelihood parameters $\{\widehat{\mathcal{A}}^{\check{\mu}}(x)\}$ contain equivalent information to the projections $\{x_{\check{\nu}}\}$ (which form jointly sufficient statistics for the amplitude parameters $\mathcal{A}$), we can use $\{\widehat{\mathcal{A}}^{\check{\mu}}\}$ as a representation of the relevant part of the data. Their sampling distribution can be written as the multivariate Gaussian

$$\mathrm{pdf}(\widehat{\mathcal{A}}|\mathcal{A}) = (\det 2\pi\mathcal{M})^{-1/2} \exp\left(-\frac{1}{2}(\widehat{\mathcal{A}}^{\check{\mu}} - \mathcal{A}^{\check{\mu}})\mathcal{M}_{\check{\mu}\check{\nu}}(\widehat{\mathcal{A}}^{\check{\nu}} - \mathcal{A}^{\check{\nu}})\right) \tag{2.18}$$

This is useful for conducting Monte Carlo simulations (as was done in [2]): one need not simulate the full GW data, only generate draws of the four maximum-likelihood parameters $\{\widehat{\mathcal{A}}^{\check{\nu}}\}$ representing the data.

It is also convenient to write the log-likelihood ratio in terms of $\widehat{\mathcal{A}}$ as well:

$$\Lambda(\mathcal{A};\widehat{\mathcal{A}}) = \mathcal{A}^{\check{\mu}}\mathcal{M}_{\check{\mu}\check{\nu}}\widehat{\mathcal{A}}^{\check{\nu}} - \frac{1}{2}\mathcal{A}^{\check{\mu}}\mathcal{M}_{\check{\mu}\check{\nu}}\mathcal{A}^{\check{\nu}} \ . \tag{2.19}$$

This is written explicitly in terms of the polar representation in Appendix B.

The $\mathcal{F}$-statistic[1] is defined as the maximized log-likelihood ratio,

$$\begin{aligned} \mathcal{F}(x) &= \max_{\mathcal{A}} \Lambda(\mathcal{A};x) = \Lambda(\widehat{\mathcal{A}};x) = \frac{1}{2}\widehat{\mathcal{A}}^{\check{\mu}}\mathcal{M}_{\check{\mu}\check{\nu}}\widehat{\mathcal{A}}^{\check{\nu}} \\ &= \frac{1}{2}I\widehat{A}_{\mathrm{R}}^2 + \frac{1}{2}J\widehat{A}_{\mathrm{L}}^2 + \widehat{A}_{\mathrm{R}}\widehat{A}_{\mathrm{L}}\left[K\sin(\widehat{\phi}_{\mathrm{R}} - \widehat{\phi}_{\mathrm{L}}) + L\cos(\widehat{\phi}_{\mathrm{R}} - \widehat{\phi}_{\mathrm{L}})\right] \end{aligned} \tag{2.20}$$

The $\mathcal{B}$-statistic[2] is defined as the Bayes factor between a model $\mathcal{H}_s$ with a signal of the form (2.11) plus (Gaussian) noise and a model $\mathcal{H}_n$ with only noise:

$$\mathcal{B}(x) = \frac{\mathrm{pdf}(x|\mathcal{H}_s)}{\mathrm{pdf}(x|\mathcal{H}_n)} = \frac{\int \mathrm{pdf}(x|\mathcal{A})\,\mathrm{pdf}(\mathcal{A}|\mathcal{H}_s)\,d^4\mathcal{A}}{\mathrm{pdf}(x|0)} = \int e^{\Lambda(\{\mathcal{A}^{\check{\mu}}\};x)}\,\mathrm{pdf}(\mathcal{A}|\mathcal{H}_s)\,d^4\mathcal{A} \tag{2.21}$$

Comparing the last form in (2.21) to the first form in (2.20), we see that while $\mathcal{F}(x)$ is constructed by maximizing the (log-)likelihood ratio over the unknown amplitude parameters, $\mathcal{B}(x)$ is made by averaging the likelihood ratio over those parameters, weighted by the prior distribution $\mathrm{pdf}(\mathcal{A}|\mathcal{H}_s)$. The prior is taken to be uniform in $\chi \in (-1,1)$, $\psi \in (-\pi/4.\pi/4)$ and $\phi_0 \in (0,2\pi)$, so that

$$\mathrm{pdf}(h_0,\chi,\psi,\phi_0|\mathcal{H}_s) = \frac{\mathrm{pdf}(h_0|\mathcal{H}_s)}{2\pi^2} \tag{2.22}$$

The convention introduced in [2] is to use an improper prior $\mathrm{pdf}(h_0|\mathcal{H}_s) = A$, $0 < h < \infty$, so that

$$\begin{aligned}\mathcal{B}(x) &= \frac{A}{2\pi^2}\int_0^{2\pi}\int_{-1}^{1}\int_{-\pi/4}^{\pi/4}\int_0^{\infty} e^{\Lambda(\{\mathcal{A}^{\check{\mu}}\};x)}\, dh_0\, d\psi\, d\chi\, d\phi_0 \\ &= \frac{A}{8\pi^2}\int_0^{2\pi}\int_0^{2\pi}\int_0^{\infty}\int_0^{\infty} e^{\Lambda(\{\mathcal{A}^{\check{\mu}}\};x)}\frac{dA_{\mathrm{R}}\, dA_{\mathrm{L}}\, d\phi_{\mathrm{R}}\, d\phi_{\mathrm{L}}}{\sqrt{A_{\mathrm{R}}A_{\mathrm{L}}}}\end{aligned} \tag{2.23}$$

Note that the prior on χ and ψ corresponds to an isotropic distribution on the source's orientation, but the prior on h_0 is an arbitrary choice motivated by convenience and mathematical simplicity.

3. An approximate form for the $\mathcal{B}$-statistic

Previous work [3] showed that the $\mathcal{B}$-statistic integral (2.23) can be exactly evaluated in the case where $K = 0 = L$, so that the metric (2.16) becomes diagonal and the left- and right-circularly polarized subspaces decouple. We show in Appendix A that K and L can be small compared to $I = J$, especially in continuous-wave observations containing an average over sidereal times and/or detectors.

When K and L are small compared to I and J, it is fruitful to consider a Taylor expansion of the $\mathcal{B}$-statistic integral (2.23), which we carry out in Appendix B, and find

$$\mathcal{B}(0) \approx \frac{A[\Gamma(\frac{1}{4})]^2}{2^{5/2}(IJ)^{1/4}} \tag{3.1}$$

and

$$\begin{aligned}\ln\frac{\mathcal{B}(x)}{\mathcal{B}(0)} \approx{}& \ln {}_1F_1\left(\frac{1}{4},1,\frac{I\widehat{A}_{\mathrm{R}}^2}{2}\right)+\ln {}_1F_1\left(\frac{1}{4},1,\frac{J\widehat{A}_{\mathrm{L}}^2}{2}\right)+\left[K\sin(\widehat{\phi}_{\mathrm{R}}-\widehat{\phi}_{\mathrm{L}})+L\cos(\widehat{\phi}_{\mathrm{R}}-\widehat{\phi}_{\mathrm{L}})\right]\widehat{A}_{\mathrm{R}}\widehat{A}_{\mathrm{L}} \\ &\times\left[\frac{1}{4}\left(\frac{{}_1F_1\left(\frac{5}{4},2,\frac{I\widehat{A}_{\mathrm{R}}^2}{2}\right)}{{}_1F_1\left(\frac{1}{4},1,\frac{I\widehat{A}_{\mathrm{R}}^2}{2}\right)}\right)+\frac{1}{4}\left(\frac{{}_1F_1\left(\frac{5}{4},2,\frac{J\widehat{A}_{\mathrm{L}}^2}{2}\right)}{{}_1F_1\left(\frac{1}{4},1,\frac{J\widehat{A}_{\mathrm{L}}^2}{2}\right)}\right)-\frac{1}{16}\left(\frac{{}_1F_1\left(\frac{5}{4},2,\frac{I\widehat{A}_{\mathrm{R}}^2}{2}\right)}{{}_1F_1\left(\frac{1}{4},1,\frac{I\widehat{A}_{\mathrm{R}}^2}{2}\right)}\right)\left(\frac{{}_1F_1\left(\frac{5}{4},2,\frac{J\widehat{A}_{\mathrm{L}}^2}{2}\right)}{{}_1F_1\left(\frac{1}{4},1,\frac{J\widehat{A}_{\mathrm{L}}^2}{2}\right)}\right)\right]\end{aligned} \tag{3.2}$$

where ${}_1F_1(a,b,z) = M(a,b,z)$ is the confluent hypergeometric function [4] and the terms omitted are second order and higher in K and/or L. It is convenient to factor out the constant $\mathcal{B}(0)$, because the detection statistic $\ln\frac{\mathcal{B}(x)}{\mathcal{B}(0)}$ is more directly comparable to $\mathcal{F}(x)$. (For example, both vanish when $x = 0$.)

We can compare this to several limiting cases and alternative forms. First, note that if $K = 0 = L$, we recover the result of section 6.1 of [3]. [See equation (6.11) of that work.] Second, in the limit that $\widehat{A}_{\mathrm{R}}$ and $\widehat{A}_{\mathrm{L}}$ are both large, the asymptotic form of

the confluent hypergeometric functions [see identity (13.5.1) of [4]]

$$ {}_1F_1\left(\frac{1}{4}, 1, \frac{I\widehat{A}^2}{2}\right) \overset{\widehat{A}\to\infty}{\longrightarrow} \frac{1}{\Gamma(\frac{1}{4})}\left(\frac{I\widehat{A}^2}{2}\right)^{-3/4} e^{I\widehat{A}^2/2} \tag{3.3a} $$

$$ {}_1F_1\left(\frac{5}{4}, 2, \frac{I\widehat{A}^2}{2}\right) \overset{\widehat{A}\to\infty}{\longrightarrow} \frac{1}{\Gamma(\frac{5}{4})}\left(\frac{I\widehat{A}^2}{2}\right)^{-3/4} e^{I\widehat{A}^2/2} \tag{3.3b} $$

says that

$$ \begin{aligned} \ln\frac{\mathcal{B}(x)}{\mathcal{B}(0)} \overset{\widehat{A}_{\mathrm{R}},\widehat{A}_{\mathrm{L}}\to\infty}{\longrightarrow} & \frac{1}{2}I\widehat{A}_{\mathrm{R}}^2 + \frac{1}{2}J\widehat{A}_{\mathrm{L}}^2 + \left[K\sin(\widehat{\phi}_{\mathrm{R}} - \widehat{\phi}_{\mathrm{L}}) + L\cos(\widehat{\phi}_{\mathrm{R}} - \widehat{\phi}_{\mathrm{L}})\right]\widehat{A}_{\mathrm{R}}\widehat{A}_{\mathrm{L}} \\ & - \frac{3}{4}\ln\left(\frac{1}{2}I\widehat{A}_{\mathrm{R}}^2\right) - \frac{3}{4}\ln\left(\frac{1}{2}J\widehat{A}_{\mathrm{L}}^2\right) - 2\ln\Gamma\left(\frac{1}{4}\right) \\ & = \mathcal{F} - \frac{3}{2}\ln(\widehat{A}_{\mathrm{R}}\widehat{A}_{\mathrm{L}}) + \text{const} \end{aligned} \tag{3.4} $$

which is the result in equation (5.37) of [3].

4. Evaluation of Approximation

We evaluate the approximation for three cases of interest, which are further detailed in Appendix A:

(i) The case originally considered in [2]: a $T_{\mathrm{obs}} = 25\,\mathrm{hr}$ observation of a source at right ascension 2 radians, declination -0.5 radians, with a single detector (LIGO Hanford, known as H1) beginning at GPS time 756950413 (2004 Jan 1 at 00:00 UTC), for which $I = J = 0.388\frac{T_{\mathrm{obs}}}{S_n(f_0)}$, $K = -0.0207\frac{T_{\mathrm{obs}}}{S_n(f_0)}$, and $L = -0.0805\frac{T_{\mathrm{obs}}}{S_n(f_0)}$. so $K/I = -0.0533$ and $L/I = -0.207$. This is a typical long-observation case.¶

(ii) An observation with perfect sidereal-time averaging of a source on the celestial equator (declination 0) using only H1. As shown in Appendix A, this is a worst-case long-observation scenario, for which $I = J = 0.305\frac{T_{\mathrm{obs}}}{S_n(f_0)}$, $K = 0$, and $L = -0.1479\frac{T_{\mathrm{obs}}}{S_n(f_0)}$. so $K/I = 0$ and $L/I = -0.485$. It provides an intermediate case where the approximation has not broken down completely.

(iii) A short two-detector (LIGO Hanford and Livingston) observation of a source at right ascension 2 radians, declination -0.5 radians, at Greenwich sidereal time 00:00, for which $I = J = 0.679\frac{T_{\mathrm{obs}}}{S_n(f_0)}$, $K = 0.1604\frac{T_{\mathrm{obs}}}{S_n(f_0)}$, and $L = 0.6527\frac{T_{\mathrm{obs}}}{S_n(f_0)}$. so $K/I = 0.236$ and $L/I = 0.961$. This is a case where we do not expect the approximation to perform well.

¶ Note that this case is slightly less favorable than another realistic alternative with the same sky position, which averages over the O1 segments from LIGO Hanford and LIGO Livingston, for which $I = J = 0.373\frac{T_{\mathrm{obs}}}{S_n(f_0)}$, $K = -0.0120\frac{T_{\mathrm{obs}}}{S_n(f_0)}$, and $L = -0.0385\frac{T_{\mathrm{obs}}}{S_n(f_0)}$. so $K/I = -0.0321$ and $L/I = -0.103$. However, as we shall see, the approximation performs well enough for the case considered that this more favorable case would be a redundant illustration.

Note that in the investigations in Appendix A, three factors tend to impact the size of L/I and K/I and the validity of the approximation:

- Observations which average roughly evenly over sidereal time suppress L/I and especially K/I. Note that this is a side effect of long observation times, but the observation time itself is not important once it exceeds one sidereal day.
- Sources closer to the poles produce a better approximation than sources closer to the equator.
- Averaging over more detectors improves the approximation.

So, although case (ii) involves perfect sidereal averaging, it is not as good an approximation as case (i) because case (ii) deliberately chooses a worst-case sky location.

4.1. Numerical Evaluation of $\mathcal{B}$-statistic Integral

To compare our approximate form of the $\mathcal{B}$-statistic to its exact value, we have to evaluate the integral (2.23). It was shown in [3] that the log-likelihood ratio (2.15) can be written in physical coordinates as

$$\Lambda(\{\mathcal{A}^{\check{\mu}}\}; x) = h_0\, \omega(x;\chi,\psi)\cos(\phi_0 - \varphi_0(x;\chi,\psi)) - \frac{h_0^2[\gamma(\chi,\psi)]^2}{2} \tag{4.1}$$

and the h_0 and ϕ_0 integrals performed explicitly to reduce the $\mathcal{B}$-statistic to a double integral[+]

$$\mathcal{B}(x) = \frac{A}{\sqrt{2\pi}} \int_{-1}^{1}\int_{-\pi/4}^{\pi/4} \frac{I_0(\zeta(x;\chi,\psi))\, e^{\zeta(x;\chi,\psi)}}{\gamma(\chi,\psi)}\, d\psi\, d\chi \ , \tag{4.2}$$

where

$$\zeta(x;\chi,\psi) = \frac{[\omega(x;\chi,\psi)]^2}{4[\gamma(\chi,\psi)]^2} \ . \tag{4.3}$$

We note here the explicit forms of $\gamma(\chi,\psi)$ and $\omega(x;\chi,\psi)$. (The form of $\varphi_0(x;\chi,\psi)$ is irrelevant to the result of the integral.) From (B.2) we can see

$$\begin{aligned}\gamma(\chi,\psi)^2 = \frac{\mathcal{A}^{\check{\mu}}\mathcal{M}_{\check{\mu}\check{\nu}}\mathcal{A}^{\check{\nu}}}{h_0^2} &= \frac{1}{h_0^2}\left[IA_{\mathrm{R}}^2 + JA_{\mathrm{L}}^2 + 2A_{\mathrm{R}}A_{\mathrm{L}}\left[K\sin(\phi_{\mathrm{R}}-\phi_{\mathrm{L}}) + L\cos(\phi_{\mathrm{R}}-\phi_{\mathrm{L}})\right]\right] \\ &= I\left(\frac{1+\chi}{2}\right)^4 + J\left(\frac{1-\chi}{2}\right)^4 + 2\left(\frac{1+\chi}{2}\right)^2\left(\frac{1-\chi}{2}\right)^2\left[K\sin(4\psi) + L\cos(4\psi)\right] \ .\end{aligned} \tag{4.4}$$

while

$$\begin{aligned}\omega(x;\chi,\psi)\cos(\phi_0 - \varphi_0(x;\chi,\psi)) &= \frac{\mathcal{A}^{\check{\mu}}x_{\check{\mu}}}{h_0} \\ &= \left(\frac{1+\chi}{2}\right)^2(x_{\check{1}}\cos\phi_{\mathrm{R}} + x_{\check{2}}\sin\phi_{\mathrm{R}}) + \left(\frac{1-\chi}{2}\right)^2(x_{\check{3}}\cos\phi_{\mathrm{L}} + x_{\check{4}}\sin\phi_{\mathrm{L}}) \\ &= U\cos\phi_0 + V\sin\phi_0\end{aligned} \tag{4.5}$$

[+] A similar reduction to a two-dimensional integral appears in [5], with the integrand empirically estimated rather than evaluated analytically.

so $[\omega(x;\chi,\psi)]^2 = U^2 + V^2$, where

$$U = \cos 2\psi \left[\left(\frac{1+\chi}{2}\right)^2 x_{\check{1}} + \left(\frac{1-\chi}{2}\right)^2 x_{\check{3}}\right] + \sin 2\psi \left[\left(\frac{1+\chi}{2}\right)^2 x_{\check{2}} - \left(\frac{1-\chi}{2}\right)^2 x_{\check{4}}\right] \tag{4.6a}$$

$$V = \cos 2\psi \left[\left(\frac{1+\chi}{2}\right)^2 x_{\check{2}} + \left(\frac{1-\chi}{2}\right)^2 x_{\check{4}}\right] - \sin 2\psi \left[\left(\frac{1+\chi}{2}\right)^2 x_{\check{1}} - \left(\frac{1-\chi}{2}\right)^2 x_{\check{3}}\right] \tag{4.6b}$$

In the simulations that follow, we evaluate the integrals for the $\mathcal{B}$-statistic using a 3000-point Monte Carlo integration on the space $\chi \in (-1, 1)$, $\psi \in (-\pi/4, \pi/4)$. This has the advantage that, even when the integrand depends only weakly on ψ, we still estimate the χ integral accurately. For 3000 points, we see Monte Carlo errors of $\mathcal{O}(1\%)$.

4.2. Comparison of Statistic Values

We compare our approximation to the numerically-evaluated exact $\mathcal{B}$-statistic, and to the $\mathcal{F}$-statistic. Each statistic is a function of the four data values $\{x_{\check{\mu}}\}$. However, if we express it in terms of the maximum-likelihood parameters $\{\widehat{\mathcal{A}}^{\check{\mu}}\}$, we see that all of the statistics are independent of the combination $\widehat{\phi}_{\mathrm{R}} + \widehat{\phi}_{\mathrm{L}} = 2\widehat{\phi}_0$ and depend on the angles $\widehat{\phi}_{\mathrm{R}}$ and $\widehat{\phi}_{\mathrm{L}}$ only in the combination $\widehat{\phi}_{\mathrm{R}} - \widehat{\phi}_{\mathrm{L}} = 4\widehat{\psi}$. Thus we can consider the statistics on the three-dimensional space parameterized by $\widehat{A}_{\mathrm{R}} \geq 0$, $\widehat{A}_{\mathrm{L}} \geq 0$, and $\widehat{\phi}_{\mathrm{R}} - \widehat{\phi}_{\mathrm{L}} \in [0, 2\pi)$. For visualization purposes, we plot contours of constant statistic versus $\widehat{A}_{\mathrm{R}}$ and $\widehat{A}_{\mathrm{L}}$ on slices of constant $\widehat{\phi}_{\mathrm{R}} - \widehat{\phi}_{\mathrm{L}}$, in analogy to Figure 3 of [3], which considered a metric with $K = 0 = L$, for which the statistics were independent of $\widehat{\phi}_{\mathrm{R}}$ and $\widehat{\phi}_{\mathrm{L}}$. If we plot $\widehat{\phi}_{\mathrm{R}} - \widehat{\phi}_{\mathrm{L}} = 0$ in the first quadrant and $\widehat{\phi}_{\mathrm{R}} - \widehat{\phi}_{\mathrm{L}} = \pi$ in the second, we are effectively plotting $\widehat{A}_{\mathrm{R}} \cos(\widehat{\phi}_{\mathrm{R}} - \widehat{\phi}_{\mathrm{L}})$ versus $\widehat{A}_{\mathrm{L}}$ on the slice $\sin(\widehat{\phi}_{\mathrm{R}} - \widehat{\phi}_{\mathrm{L}}) = 0$. Likewise, if we plot $\widehat{\phi}_{\mathrm{R}} - \widehat{\phi}_{\mathrm{L}} = \frac{\pi}{2}$ in the first quadrant and $\widehat{\phi}_{\mathrm{R}} - \widehat{\phi}_{\mathrm{L}} = -\frac{\pi}{2}$ in the second, we are effectively plotting $\widehat{A}_{\mathrm{R}} \sin(\widehat{\phi}_{\mathrm{R}} - \widehat{\phi}_{\mathrm{L}})$ versus $\widehat{A}_{\mathrm{L}}$ on the slice $\cos(\widehat{\phi}_{\mathrm{R}} - \widehat{\phi}_{\mathrm{L}})$. Since the approximate $\mathcal{B}$-statistic and the $\mathcal{F}$-statistic both depend on the combination $K\sin(\phi_{\mathrm{R}} - \phi_{\mathrm{L}}) + L\cos(\phi_{\mathrm{R}} - \phi_{\mathrm{L}})$, the former slice focuses on the impact of L and the second on the impact of K. Note that another choice of slice would be to chose $\phi_{\mathrm{R}} - \phi_{\mathrm{L}} = \tan^{-1}\left(-\frac{L}{K}\right)$, so that the K-and-L-dependent part of the statistics vanished, or $\phi_{\mathrm{R}} - \phi_{\mathrm{L}} = \tan^{-1}\left(\frac{K}{L}\right)$, which would maximize the impact of this term. In practice, for the examples we chose, $|L|$ is significantly larger than $|K|$, so these slices would be similar to the ones we plot.

We choose our contours for these plots to correspond to specific false-alarm probabilities (estimated by drawing 10^7 random points $\{\widehat{\mathcal{A}}^{\check{\mu}}\}$ from a Gaussian with zero mean and variance-covariance matrix $\{\mathcal{M}^{\check{\mu}\check{\nu}}\}$) rather than specific statistic values. In figure 1, we see that for the case (i), with $K/I = -0.0533$ and $L/I = -0.207$, the approximation works well and the approximate and exact $\mathcal{B}$-statistic contours are nearly indistinguishable. Figure 2 shows case (ii), for which $K/I = 0$ and $L/I = -0.485$. Some discrepancy is visible for low false-alarm rates when the maximum-likelihood value corresponds to linear polarization with $\widehat{\psi} \approx 0$, i.e., $\widehat{A}_{\mathrm{R}} e^{i\widehat{\phi}_{\mathrm{R}}} \approx \widehat{A}_{\mathrm{L}} e^{i\widehat{\phi}_{\mathrm{L}}}$. Finally, in figure 3

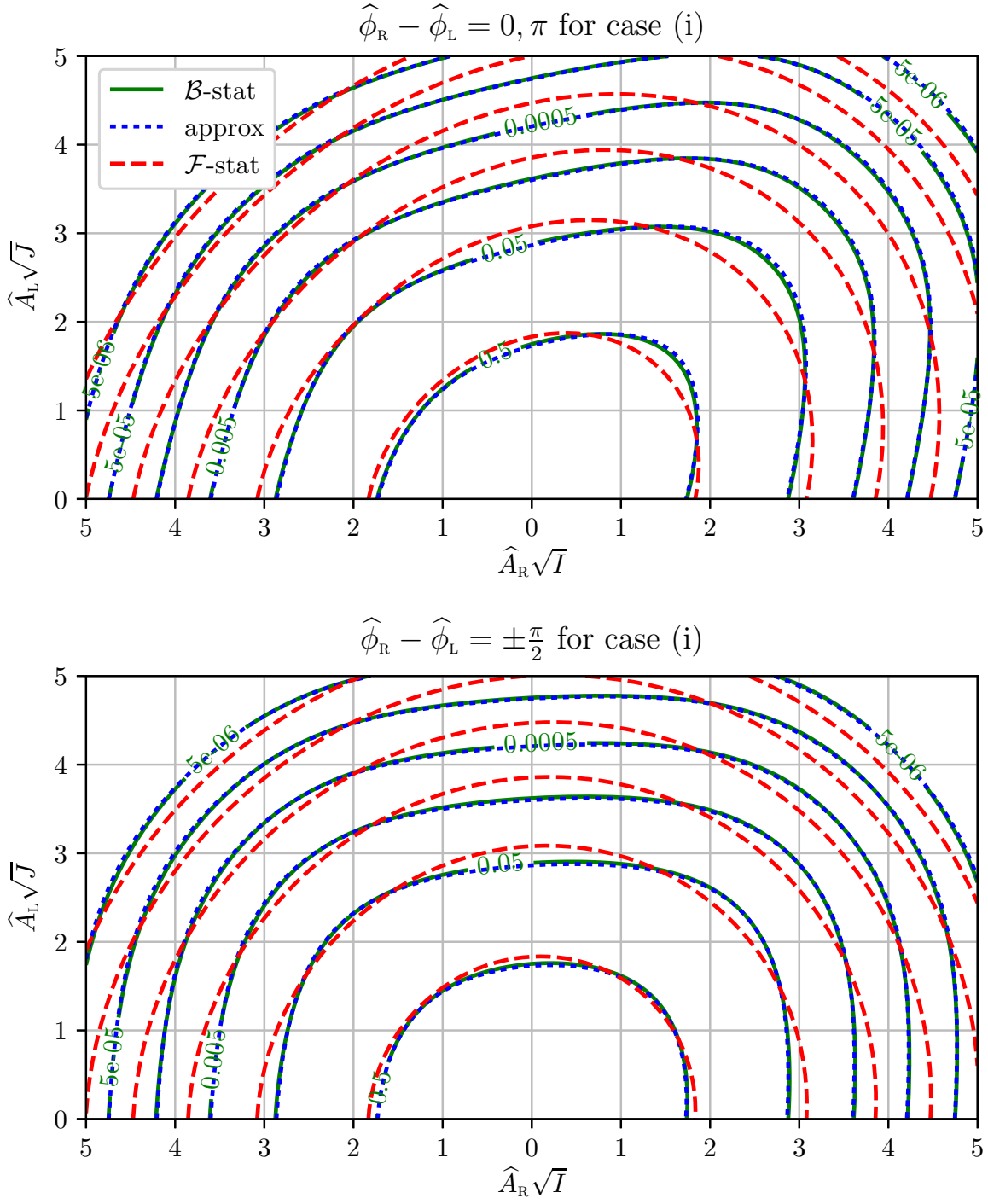

Figure 1. Comparison of $\mathcal{B}$-statistic (2.23) and approximation (3.2), along with $\mathcal{F}$-statistic (2.20); using the assumptions of a 25-hour observation beginning 2004 Jan 1 at 00:00 UTC (GPS time 756950413) [case (i)], for which $K/I = -0.0533$ and $L/I = -0.207$. The statistics depend on the data through the maximum-likelihood parameters $\widehat{A}_{\rm R}$, $\widehat{A}_{\rm L}$, and $\widehat{\phi}_{\rm R} - \widehat{\phi}_{\rm L}$. Top: the slice $\sin(\widehat{\phi}_{\rm R} - \widehat{\phi}_{\rm L}) = 0$, for which the L-dependent terms of the statistics are important; bottom: the slice $\cos(\widehat{\phi}_{\rm R} - \widehat{\phi}_{\rm L}) = 0$, for which the K-dependent terms of the statistics are important. The contours of constant exact and approximate statistic are nearly indistinguishable, indicating that this is a good approximation for these metric values.

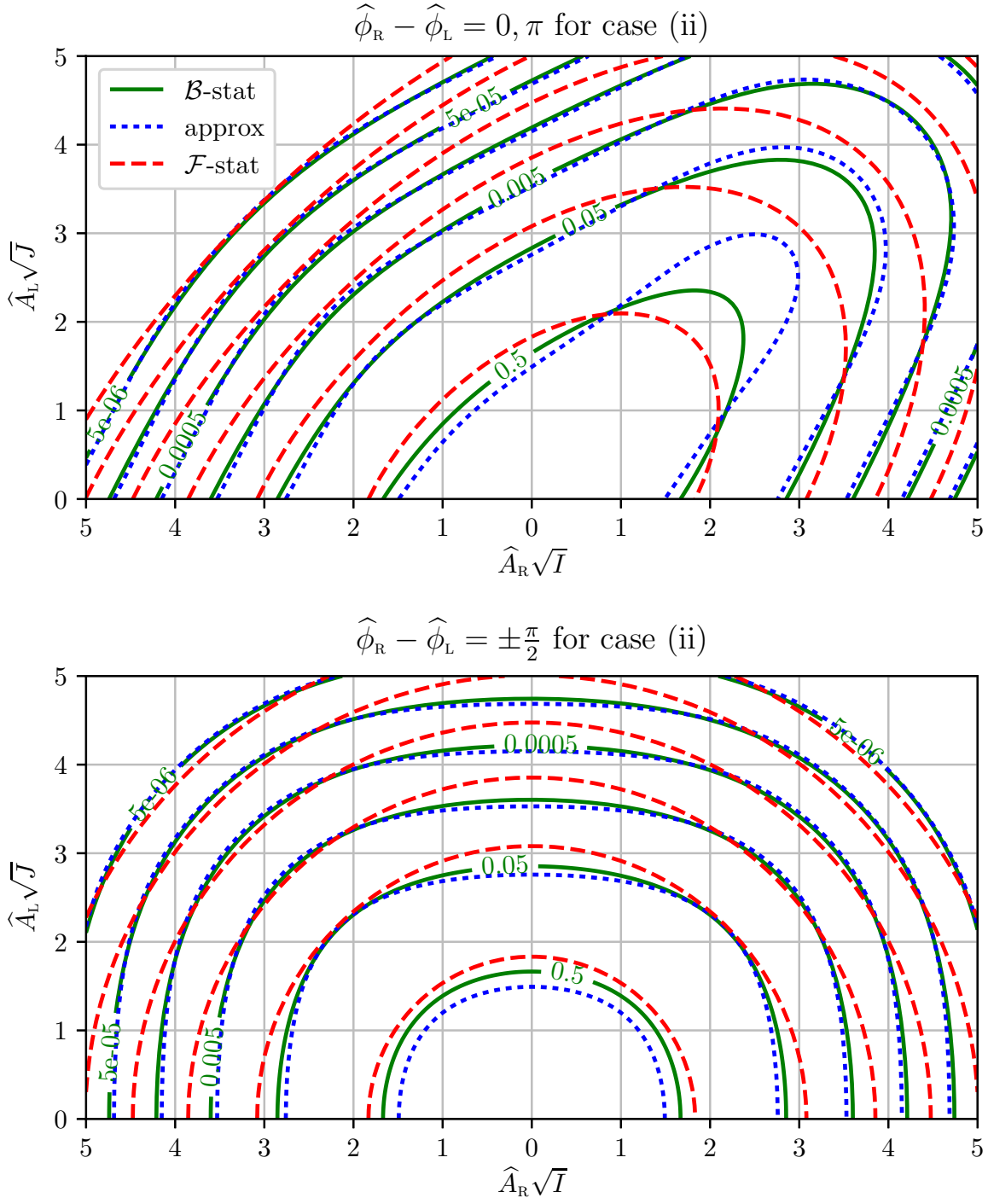

Figure 2. Comparison of $\mathcal{B}$-statistic and approximation, along with $\mathcal{F}$-statistic, assuming a source on the celestial equator and H1 observations which evenly sample sidereal time [case (ii)], for which $K/I = 0$ and $L/I = -0.485$, contours and slices constructed as in figure 1. There is some discrepancy between the approximate and exact $\mathcal{B}$-statistic contours at low false alarm rate in the case of linear polarization $\widehat{A}_{\mathrm{R}} \approx \widehat{A}_{\mathrm{L}}$. Note that the disagreement for this contour in other directions is because it is drawn at the same false alarm probability, so the approximate $\mathcal{B}$-statistic contour must be inside the exact $\mathcal{B}$-statistic contour to compensate for the deformation in one direction.

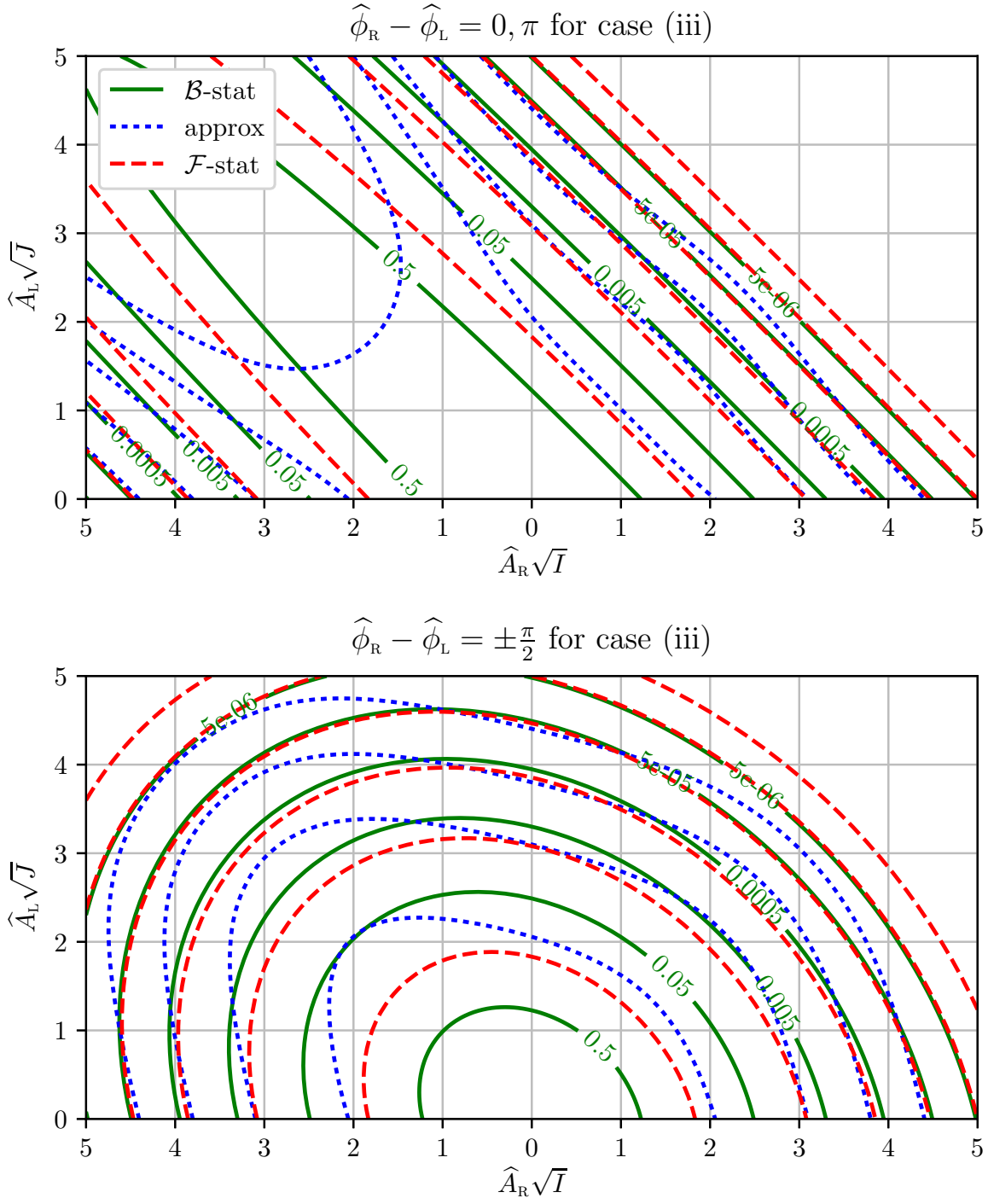

Figure 3. Comparison of $\mathcal{B}$-statistic and approximation, along with $\mathcal{F}$-statistic, assuming a single Greenwich sidereal time of 00:00 [case (iii)], for which $K/I = 0.236$ and $L/I = 0.961$, contours and slices constructed as in figure 1. Now the contours for the approximate $\mathcal{B}$-statistic are quite far off of those of the exact $\mathcal{B}$-statistic. In fact, the entirety of both plots lie above the median of the approximate $\mathcal{B}$-statistic under the no-signal hypothesis; the contour in the upper left of the top plot is a false alarm probability of 0.05, and the one in the center of the lower plot is 0.0005. The origin $\widehat{A}_{\rm R} = 0 = \widehat{A}_{\rm L}$ is at the 98th percentile of the approximate $\mathcal{B}$-statistic, but the minimum of the exact $\mathcal{B}$-statistic. Thus the approximation is, as expected, inappropriate for a value of $\sqrt{K^2 + L^2}/I$ so close to unity.

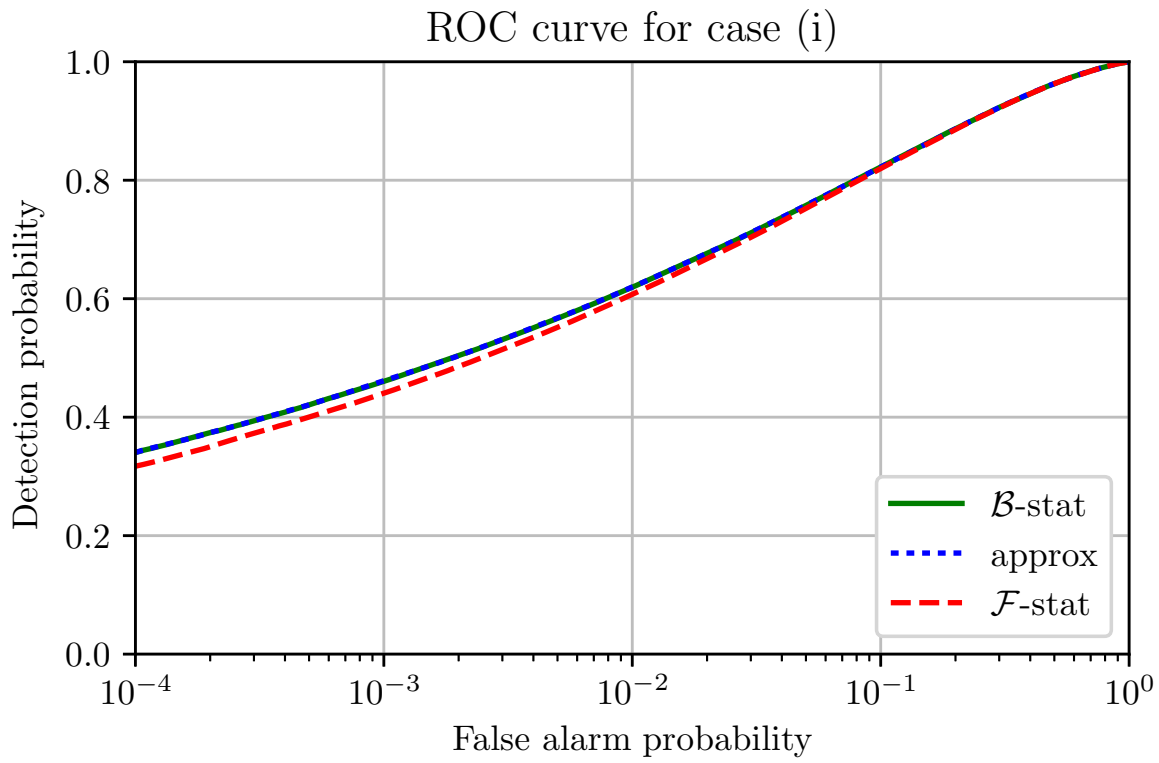

Figure 4. ROC curves for $\mathcal{B}$-statistic and approximation, along with $\mathcal{F}$-statistic, using the metric from case (i) (see figure 1). In this case, the approximate $\mathcal{B}$-statistic performs identically to the exact one. Compare figure 3 of [2].

we show the case (iii), with $K/I = 0.236$ and $L/I = 0.961$. The approximation performs badly, as we'd expect for a first-order expansion in a quantity close to unity.

4.3. Monte Carlo Simulations

To evaluate the performance of our $\mathcal{B}$-statistic approximation, we produced Monte Carlo simulations by drawing 10^6 sets of signal parameters, using a fixed value of $h_0 = 10\frac{S_n(f_0)}{T_{\rm obs}}$ and drawing the parameters χ, ψ, and ϕ_0 from uniform distributions. Each of these sets of parameters was converted into a point $\mathcal{A}^{\check{\mu}}$, and then a signal $\widehat{\mathcal{A}}^{\check{\mu}}$ was generated by drawing from a Gaussian with mean $\mathcal{A}^{\check{\mu}}$ and variance-covariance matrix $\{\mathcal{M}^{\check{\mu}\check{\nu}}\}$. A receiver-operating-characteristic (ROC) curve was generated for each statistic by plotting the fraction of signal points above a signal threshold (detection probability) against the fraction of noise points (described in the previous section) above the same threshold. The latter fraction is known as false-alarm probability, Type I error probability, or, in the language of hypothesis testing, significance. A superior detection statistic will have a higher detection efficiency at a given false-alarm probability, and thus be found above and to the left of an inferior one. Note that while an extension of the Neyman-Pearson lemma due to Searle[6] states that the Bayes factor will be the

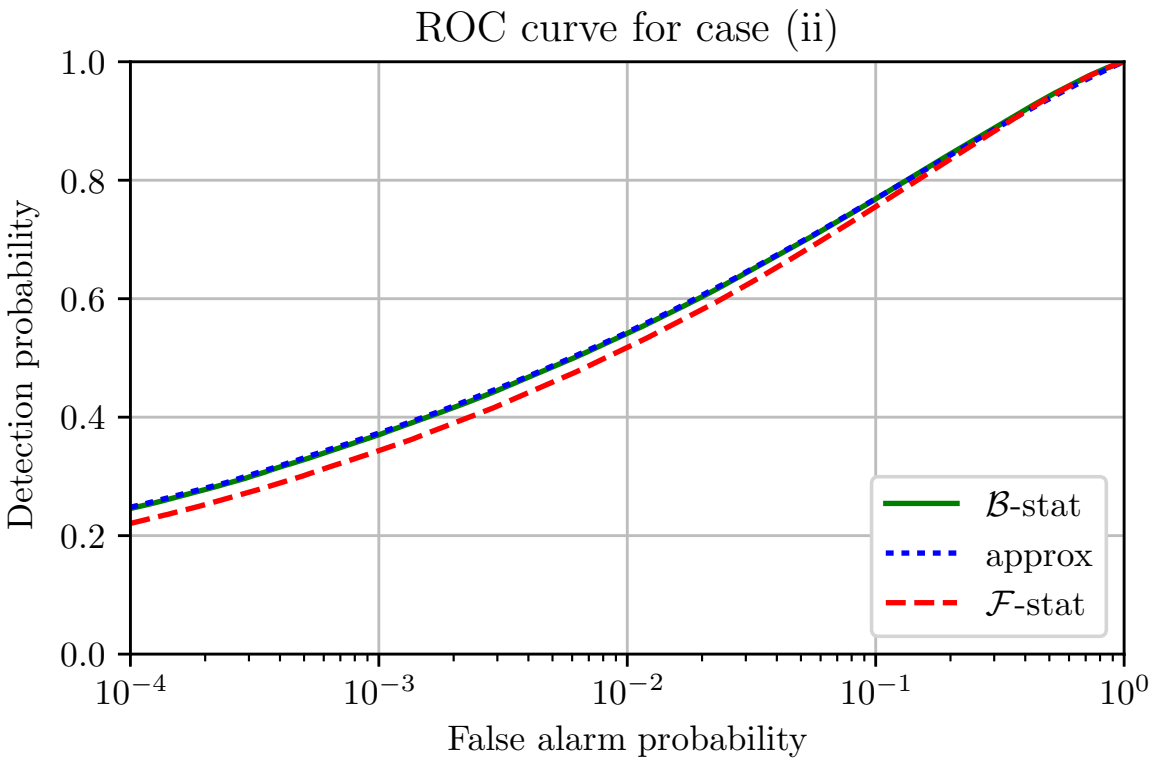

Figure 5. ROC curves for $\mathcal{B}$-statistic and approximation, along with $\mathcal{F}$-statistic, using the metric from case (ii) (see figure 2). Even though $K/I = 0$ and $L/I = -0.485$, the approximate $\mathcal{B}$-statistic, which is Taylor expanded in K/I and L/I, still performs as well as the exact $\mathcal{B}$-statistic (and better than the $\mathcal{F}$-statistic) in this Monte Carlo.

optimal test statistic for a Monte Carlo using the same prior, this is not guaranteed to be the case here, since the delta-function prior on h_0 is not the same as the uniform prior used in defining the statistic.

In figure 4 we show the ROC curve for case (i), in which our approximation was shown to match the exact $\mathcal{B}$-statistic well (see figure 1). As expected, the approximate $\mathcal{B}$-statistic performs as well as the exact one, and both outperform the $\mathcal{F}$-statistic, as shown in [2]. In figure 5 we show the ROC curve for case (ii), where our approximation was shown in figure 2 to have some discrepancies with the exact $\mathcal{B}$-statistic. Nonetheless, we see that it again performs as well as the exact $\mathcal{B}$-statistic and better than the $\mathcal{F}$-statistic. In figure 6 we show the ROC curve for case (iii), where our approximation was shown in figure 3 to disagree considerably with the exact $\mathcal{B}$-statistic. Unsurprisingly, we find this approximation to be a poor detection statistic in this scenario, underperforming both the exact $\mathcal{B}$-statistic and the $\mathcal{F}$-statistic.

4.4. Computation Time

.

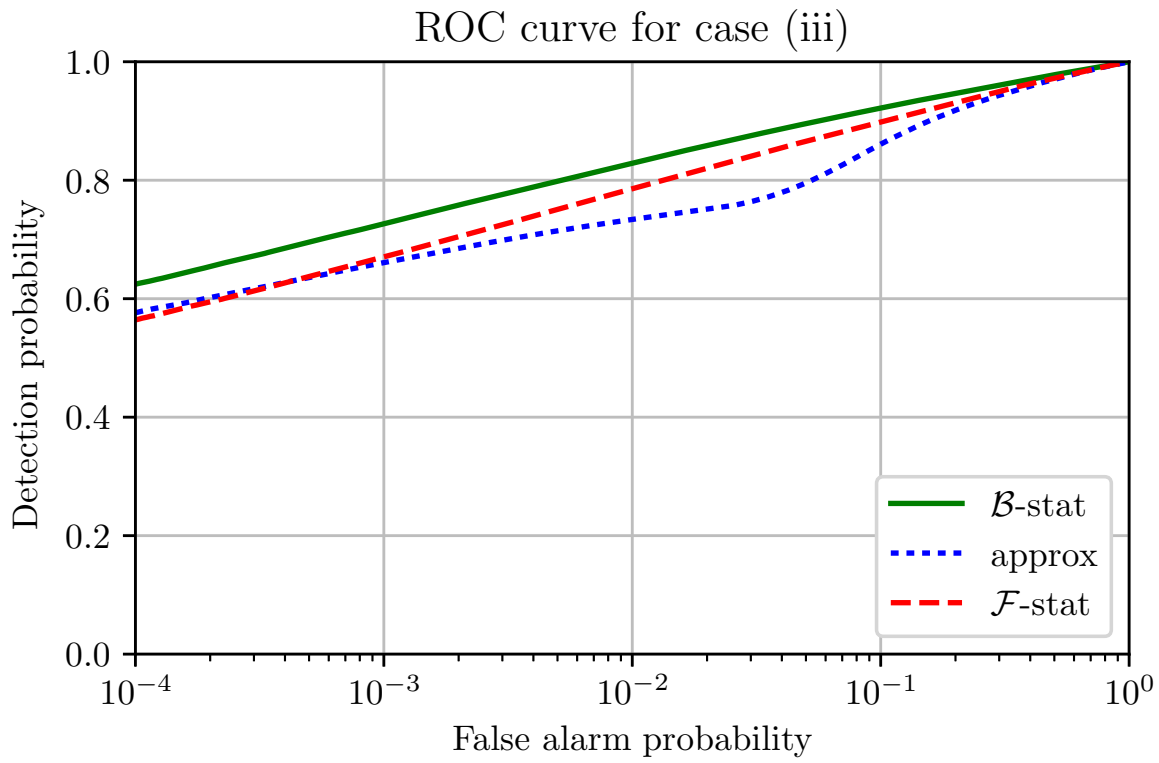

Figure 6. Comparison of $\mathcal{B}$-statistic and approximation, along with $\mathcal{F}$-statistic, using the metric from case (iii) (see figure 3). Here $K/I = 0.236$ and $L/I = 0.961$, and we see indeed that the approximate $\mathcal{B}$-statistic performs poorly, considerably below both the exact $\mathcal{B}$-statistic and the $\mathcal{F}$-statistic.

A comprehensive study of the computation time of the three statistics ($\mathcal{F}$-statistic, numerically-evaluated $\mathcal{B}$-statistic and $\mathcal{B}$-statistic approximation) is beyond the scope of this project, but we report here some timing statistics based on the computations used to produce the plots for this paper. The computation was done in Python, using the Scientific Python libraries [7]. One should avoid reading too much into the exact quantitative computing cost, given that 1) the Monte Carlo integration to evaluate the numerical $\mathcal{B}$-statistic was not exhaustively optimized, and 2) the multi-dimensional arrays used in the Monte Carlo integration were too large to fit in memory, and so had to be broken into pieces which were looped over. Note that because the $\mathcal{F}$-statistic and the approximate $\mathcal{B}$-statistic are computed using many of the same quantities, the standard version of the code computes them together in one function. However, an additional test was done with the two in separate functions.

The timing measurements are summarized in table 1. The combined $\mathcal{F}$-statistic and approximate $\mathcal{B}$-statistic computation took $\mathcal{O}(1 - 2\ \mu\text{s})$ per evaluation, while the numerical integration for the exact $\mathcal{B}$-statistic took $\mathcal{O}(1\,\text{ms})$ per evaluation. A separate test indicates that most of the cost of the former function is in the approximate $\mathcal{B}$-statistic computation.

Table 1. Results of timing measurements. The Monte Carlo simulations for this paper included some runs with 10^6 and some runs with 10^7 evaluations of the various functions. The standard code included one function which calculated the $\mathcal{F}$-statistic (2.20) together with the approximate $\mathcal{B}$-statistic (3.2), and another which computed (by 3000-point Monte Carlo integration) the "exact" $\mathcal{B}$-statistic integral (2.23). The combined $\mathcal{F}$-statistic and approximate $\mathcal{B}$-statistic computation took $\mathcal{O}(1-2\,\mu\text{s})$ per evaluation, while the numerical integration for the exact $\mathcal{B}$-statistic took $\mathcal{O}(1\,\text{ms})$ per evaluation. A separate test indicates that most of the cost of the former function is in the approximate $\mathcal{B}$-statistic computation. Note that the absolute numbers are not meant to be definitive, as described in the text.

Function	# runs (10^6 calcs)	# runs (10^7 calcs)	median time/calcs (µs)
$\mathcal{F}$ & approx $\mathcal{B}$	7	6	0.94
$\mathcal{F}$	6	6	0.04
approx $\mathcal{B}$	6	6	0.63
numerical $\mathcal{B}$	7	7	943.89

Implementation of the $\mathcal{B}$-statistic approximation in the LSC Algorithms Library [8] is planned for the future. One potential challenge is that the approximate $\mathcal{B}$ statistic is expressed in terms of confluent hypergeometric functions, which may be more time-consuming to evaluate than the algebraic functions involved in the $\mathcal{F}$-statistic, as indicated by the Python tests presented here. Additionally, direct evaluation of these confluent hypergeometric functions for large-amplitude signals can produce overflow, even though the final approximation in terms of their logarithms and ratios may be well-behaved. It may be necessary to supplement standard library functions with strategic use of asymptotic forms.

5. Conclusions

We have produced an analytic approximation to the $\mathcal{B}$-statistic, a Bayesian detection statistic for continuous gravitational waves based on a Bayes factor between signal and noise hypotheses. This approximation is based on a Taylor expansion in the parameters K/I and L/I, which are related to observation-averaged combinations of antenna patterns, and depend on the sky position of the source, detectors involved in the observation, and distribution of the observations in sidereal time. For observations which average over a range of sidereal times, these parameters tend to be small enough to produce a good first-order approximation, and we showed via Monte Carlo simulations that the approximate statistic performed as well as the exact $\mathcal{B}$-statistic, even for a case with an expansion parameter approaching 50%. The approximation is shown to break down for observations at a single sidereal time, which indicates the approximation is not likely to be an appropriate statistic for transient modelled signals such as compact binary inspiral.

Unlike the exact $\mathcal{B}$-statistic, which must be evaluated via a two-dimensional numerical integral, our approximation (like the maximum-likelihood $\mathcal{F}$-statistic) can

be evaluated analytically, which should make it computationally more efficient, as illustrated in section 4.4. This, combined with the better detection efficiency than the $\mathcal{F}$-statistic at the same false alarm rate, makes it a potentially useful replacement for, or alternative to, the $\mathcal{F}$-statistic in a semicoherent search which combines $\mathcal{F}$-statistic values at a range of signal parameters.

Acknowledgments

We wish to thank Reinhard Prix, as well as the members of the LIGO Scientific Collaboration and Virgo Collaboration continuous waves group, for useful feedback. This work was supported by NSF grants PHY-1505629 and PHY-1806824. This paper has been assigned LIGO Document Number LIGO-P1800060-x6.

Appendix A. Form and Behavior of the Metric Elements

Given some nearly monochromatic GW signal around frequency f_0, the multi-detector scalar product of two time series x and y, used in the definition (2.16), can be expressed as

$$(x|y) \equiv \sum_{Xl} \frac{4}{S_l^X(f_0)} \,\mathrm{Re} \int_0^\infty \widetilde{x}_l^{X*}(f)\, \widetilde{y}_l^X(f)\, df \ , \tag{A.1}$$

where $S_l^X(f_0)$ is the one-sided noise power spectral density around the frequency f_0 in detector X during time stretch l, and $\widetilde{x}_l^X(f), \widetilde{y}_l^X(f)$ are the corresponding Fourier-transforms of $x^X(t), y^X(t)$ restricted to the time stretch l. This assumes the data from each detector X has been divided into short stretches of data $[t_l,\, t_l + T_{\mathrm{sft}})$ of length T_{sft}.

The metric components can be written as

$$I = A + B + 2E \quad \text{and} \quad J = A + B - 2E \quad \text{and} \quad K = 2C \quad \text{and} \quad L = A - B \tag{A.2}$$

where, in the long-wavelength limit,

$$A = \sum_{Xl} \frac{T_{\mathrm{sft}}}{S_l^X(f_0)} \left(a_l^X\right)^2 \quad \text{and} \quad B = \sum_{Xl} \frac{T_{\mathrm{sft}}}{S_l^X(f_0)} \left(b_l^X\right)^2 \quad \text{and} \quad C = \sum_{Xl} \frac{T_{\mathrm{sft}}}{S_l^X(f_0)} a_l^X b_l^X \tag{A.3}$$

and $E = 0$ (so that $I = J$). As shown in [3], the more general expression, with a complex frequency-dependent detector tensor $\overleftrightarrow{d}(f)$ and amplitude-modulation coefficients $a(f)$ and $b(f)$, the (real) metric components can be more generally written as*

$$I = \sum_{Xl} \frac{T_{\mathrm{sft}}}{S_l^X(f_0)} \left|a_l^X(f_0) - i b_l^X(f_0)\right|^2 \quad \text{and} \quad J = \sum_{Xl} \frac{T_{\mathrm{sft}}}{S_l^X(f_0)} \left|a_l^X(f_0) + i b_l^X(f_0)\right|^2 \tag{A.4a}$$

$$L + iK = \sum_{Xl} \frac{T_{\mathrm{sft}}}{S_l^X(f_0)} \left[a_l^X(f_0) - i b_l^X(f_0)\right]^* \left[a_l^X(f_0) + i b_l^X(f_0)\right] \tag{A.4b}$$

* Note that equation (A.3b) of [3] has the formulas for K and L reversed.

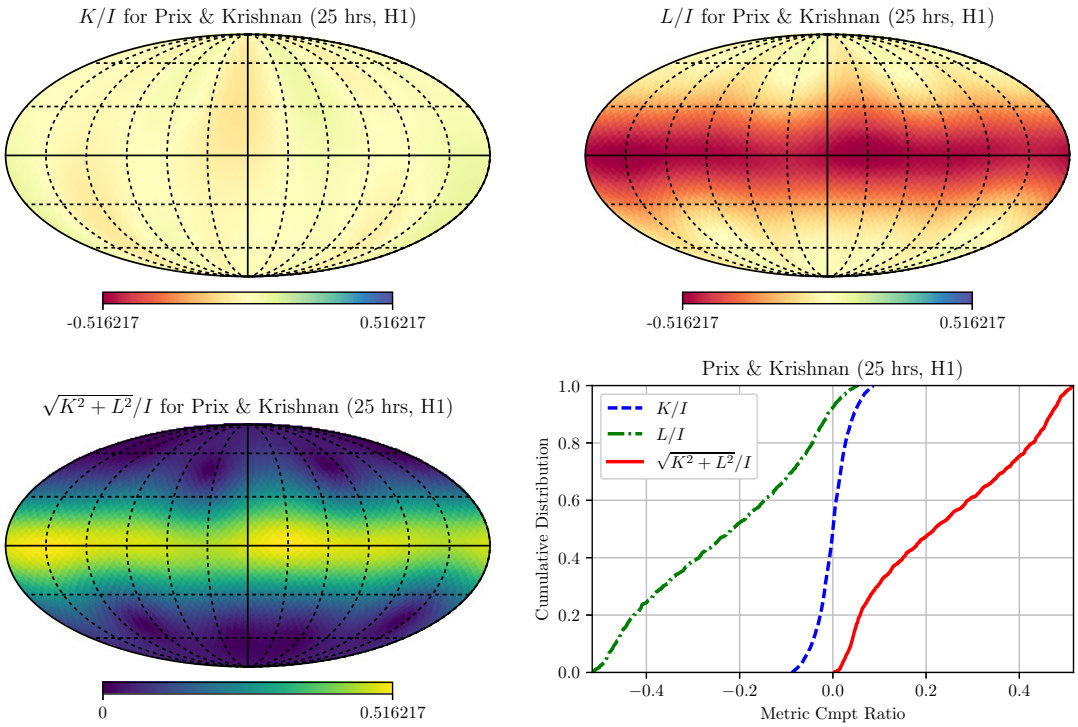

Figure A1. Plots of the metric element ratios K/I, L/I, and $\sqrt{K^2+L^2}/I$ versus sky position of targeted source, along with cumulative probability distributions of these ratios, assuming a randomly chosen sky location, using the assumption of a 25-hour observation with LIGO Hanford Observatory (H1) beginning 2004 Jan 1 at 00:00 UTC (GPS time 756950413).

In this form, we can see that the Cauchy-Schwarz inequality implies that

$$K^2 + L^2 = |L + iK|^2 \leq IJ \; ; \tag{A.5}$$

in the long-wavelength case, this becomes $\sqrt{K^2+L^2} \leq I = J$.

Prix and Krishnan [2] give an example of a $T_{\mathrm{obs}} = 25\,\mathrm{hr}$ observation of a source at right ascension 2 radians, declination -0.5 radians, with a single detector (LIGO Hanford, known as H1) beginning at GPS time 756950413 (2004 Jan 1 at 00:00 UTC) and obtain metric components of values of $A = 0.154\frac{T_{\mathrm{obs}}}{S_n(f_0)}$, $B = 0.234\frac{T_{\mathrm{obs}}}{S_n(f_0)}$, and $C = -0.0104\frac{T_{\mathrm{obs}}}{S_n(f_0)}$, which is equivalent to $I = J = 0.388\frac{T_{\mathrm{obs}}}{S_n(f_0)}$, $K = -0.0207\frac{T_{\mathrm{obs}}}{S_n(f_0)}$, and $L = -0.0805\frac{T_{\mathrm{obs}}}{S_n(f_0)}$. or $K/I = -0.0533$, $L/I = -0.207$. We explore the robustness of those ratios in figure A1, which calculated them for the same observing time and different sky positions. The ratio K/I is small (< 0.10) everywhere, while the ratio L/I is smaller away from the celestial equator.

As an alternative to the arbitrarily chosen 25-hour observing time of [2], we can consider the idealization that a long observation will include roughly the same amount of data from each sidereal time, and construct the corresponding metric components for this case. Under this idealization, the metric components will be independent of right

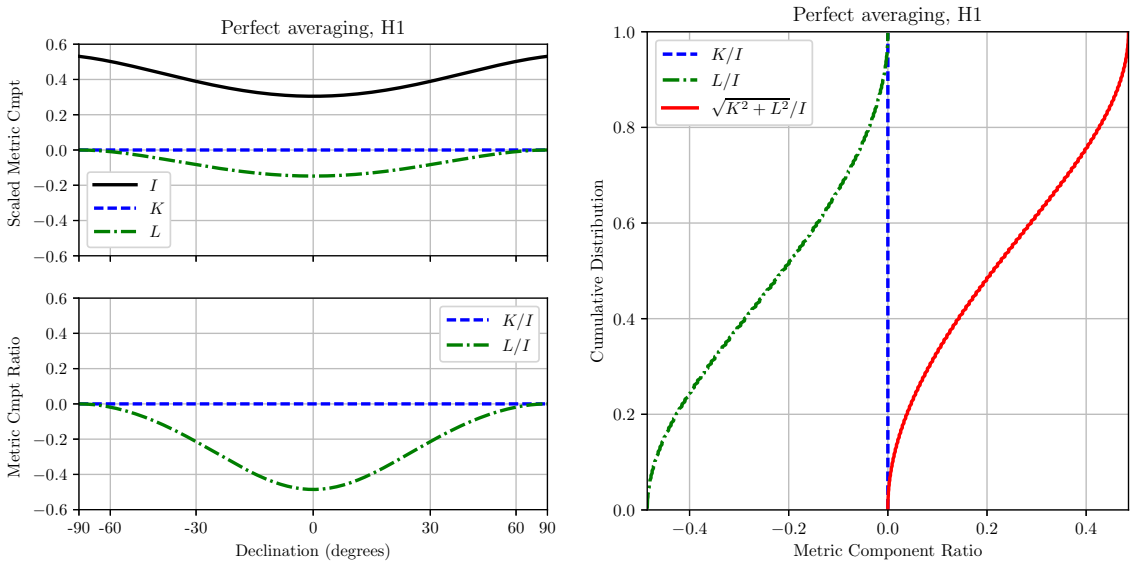

Figure A2. Left: Plots of metric elements I, K, and L, and the ratios K/I and L/I versus declination of targeted source, assuming an observation using LIGO Hanford Observatory (H1) that results in a perfect average over sidereal time. The spacing in declination is chosen to be proportional to sky area. Right: Cumulative probability distributions of the metric element ratios K/I, L/I, and $\sqrt{K^2+L^2}/I$ for this case, assuming a randomly chosen sky location.

ascension, allowing us to simply plot them versus declination. In figure A2 we plot the metric elements and their ratios versus declination. We find, as in figure A1, the ratio L/I can approach 0.50 near the celestial equator. However, this is specific to the choice of single-detector observations with H1 only. If we assume equal amounts of data from LIGO Hanford (H1) and LIGO Livingston (L1), we find that $L/I \lesssim 0.15$ over the entire sky, as shown in figure A3. We also notice that $K = 0$ for this choice of observing time. This is a geometrical result related to the symmetries of the quantity $a^X b^X$ under rotations of the Earth.

To give a more realistic example of a typical observing time, we consider the H1 and L1 segments associated with advanced LIGO's first observing run (O1)♯, from the LIGO Open Science Center[9]. We see that the ratios K/I and L/I, plotted in figure A4, are small enough that a Taylor expansion should be promising.

As a worst-case example (and an illustration of why this approximation is better suited to continuous-wave observations than to transients), in figure A5, we show the relevant metric component ratios for an observation at a single time, assumed to correspond to sidereal time 00:00 at the prime meridian. We see that in this case, the bound $\sqrt{K^2+L^2} \leq I$ is nearly saturated for much of the sky.

♯ https://doi.org/10.7935/K57P8W9D

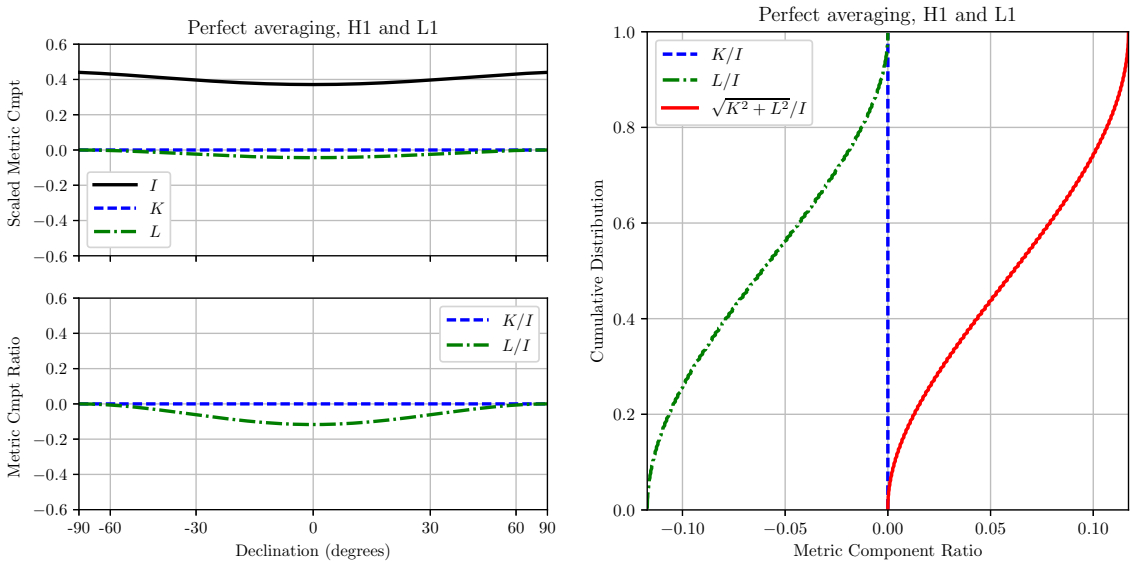

Figure A3. Left: Plots of metric elements I, K, and L, and the ratios K/I and L/I versus declination of targeted source, assuming an observation using LIGO Hanford Observatory (H1) and LIGO Livingston Observatory (L1) that results in a perfect average over sidereal time. The spacing in declination is chosen to be proportional to sky area. Right: Cumulative probability distributions of the metric element ratios K/I, L/I, and $\sqrt{K^2+L^2}/I$ for this case, assuming a randomly chosen sky location.

Appendix B. Derivation of Taylor Expansion

Here we collect the detailed derivation of the Taylor-expanding $\mathcal{B}$-statistic.

In terms of the polar representation,

$$\begin{aligned}\mathcal{A}^{\check{\mu}}\mathcal{M}_{\check{\mu}\check{\nu}}\widehat{\mathcal{A}}^{\check{\nu}} &= IA_{\mathrm{R}}\widehat{A}_{\mathrm{R}}\cos(\phi_{\mathrm{R}}-\widehat{\phi}_{\mathrm{R}}) + JA_{\mathrm{L}}\widehat{A}_{\mathrm{L}}\cos(\phi_{\mathrm{L}}-\widehat{\phi}_{\mathrm{L}})\\ &+A_{\mathrm{R}}\widehat{A}_{\mathrm{L}}\left[K\sin(\phi_{\mathrm{R}}-\widehat{\phi}_{\mathrm{L}})+L\cos(\phi_{\mathrm{R}}-\widehat{\phi}_{\mathrm{L}})\right]+A_{\mathrm{L}}\widehat{A}_{\mathrm{R}}\left[-K\sin(\phi_{\mathrm{L}}-\widehat{\phi}_{\mathrm{R}})+L\cos(\phi_{\mathrm{L}}-\widehat{\phi}_{\mathrm{R}})\right]\end{aligned} \tag{B.1}$$

and [see eqn (5.10) of [3]]

$$\mathcal{A}^{\check{\mu}}\mathcal{M}_{\check{\mu}\check{\nu}}\mathcal{A}^{\check{\nu}} = IA_{\mathrm{R}}^2 + JA_{\mathrm{L}}^2 + 2A_{\mathrm{R}}A_{\mathrm{L}}\left[K\sin(\phi_{\mathrm{R}}-\phi_{\mathrm{L}})+L\cos(\phi_{\mathrm{R}}-\phi_{\mathrm{L}})\right] \tag{B.2}$$

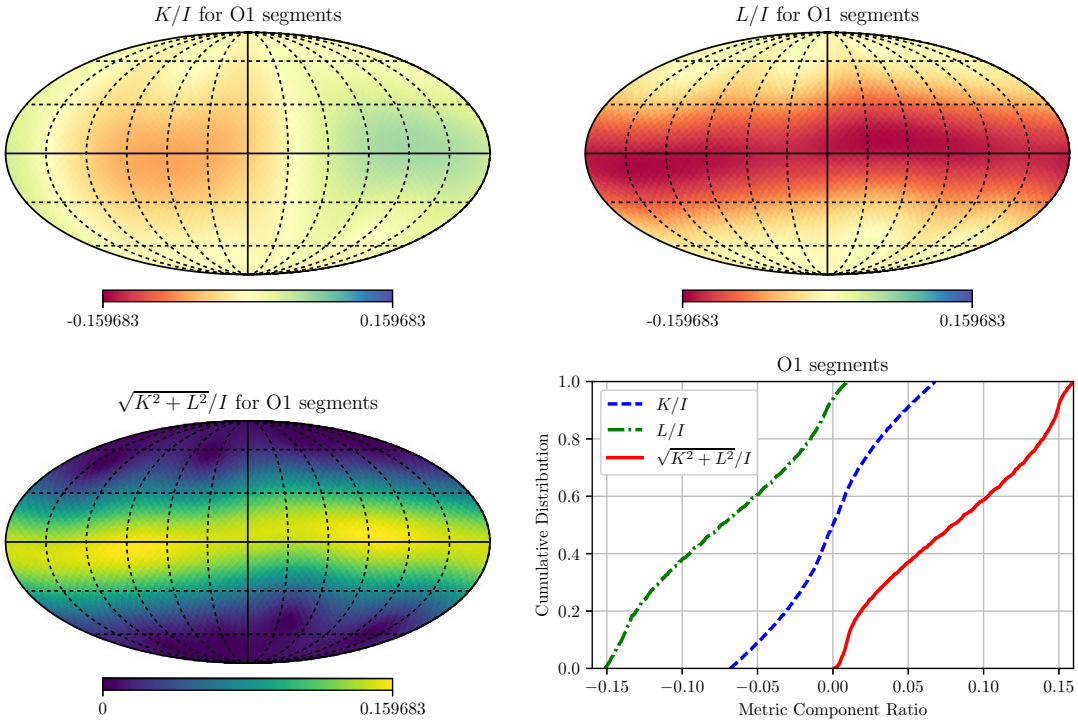

Figure A4. Plots of the metric element ratios K/I, L/I, and $\sqrt{K^2+L^2}/I$ versus sky position of targeted source, along with cumulative probability distributions of these ratios, assuming a randomly chosen sky location, for an observation corresponding to the data segments (H1 and L1) from Advanced LIGO's first observing run (O1).

so that

$$
\begin{aligned}
\Lambda(\mathcal{A};x) = {} & I\left(-\frac{1}{2}A_{\mathrm{R}}^2 + A_{\mathrm{R}}\widehat{A}_{\mathrm{R}}\cos(\phi_{\mathrm{R}}-\widehat{\phi}_{\mathrm{R}})\right) + J\left(-\frac{1}{2}A_{\mathrm{L}}^2 + A_{\mathrm{L}}\widehat{A}_{\mathrm{L}}\cos(\phi_{\mathrm{L}}-\widehat{\phi}_{\mathrm{L}})\right) \\
& + K\left(-A_{\mathrm{R}}A_{\mathrm{L}}\sin(\phi_{\mathrm{R}}-\phi_{\mathrm{L}}) + A_{\mathrm{R}}\widehat{A}_{\mathrm{L}}\sin(\phi_{\mathrm{R}}-\widehat{\phi}_{\mathrm{L}}) - \widehat{A}_{\mathrm{R}}A_{\mathrm{L}}\sin(\phi_{\mathrm{L}}-\widehat{\phi}_{\mathrm{R}})\right) \\
& + L\left(-A_{\mathrm{R}}A_{\mathrm{L}}\cos(\phi_{\mathrm{R}}-\phi_{\mathrm{L}}) + A_{\mathrm{R}}\widehat{A}_{\mathrm{L}}\cos(\phi_{\mathrm{R}}-\widehat{\phi}_{\mathrm{L}}) + \widehat{A}_{\mathrm{R}}A_{\mathrm{L}}\cos(\phi_{\mathrm{L}}-\widehat{\phi}_{\mathrm{R}})\right) \\
= {} & \Lambda_{\mathrm{R}}(A_{\mathrm{R}},\phi_{\mathrm{R}};\widehat{A}_{\mathrm{R}},\widehat{\phi}_{\mathrm{R}}) + \Lambda_{\mathrm{L}}(A_{\mathrm{L}},\phi_{\mathrm{L}};\widehat{A}_{\mathrm{L}},\widehat{\phi}_{\mathrm{L}}) \\
& + \left[K\sin(\widehat{\phi}_{\mathrm{R}}-\widehat{\phi}_{\mathrm{L}}) + L\cos(\widehat{\phi}_{\mathrm{R}}-\widehat{\phi}_{\mathrm{L}})\right] \\
& \quad \times \left[A_{\mathrm{R}}A_{\mathrm{L}}\left(-\cos(\phi_{\mathrm{R}}-\widehat{\phi}_{\mathrm{R}})\cos(\phi_{\mathrm{R}}-\widehat{\phi}_{\mathrm{R}}) + \sin(\phi_{\mathrm{R}}-\widehat{\phi}_{\mathrm{R}})\sin(\phi_{\mathrm{L}}-\widehat{\phi}_{\mathrm{L}})\right)\right. \\
& \qquad \left. + A_{\mathrm{R}}\widehat{A}_{\mathrm{L}}\cos(\phi_{\mathrm{R}}-\widehat{\phi}_{\mathrm{R}}) + \widehat{A}_{\mathrm{R}}A_{\mathrm{L}}\cos(\phi_{\mathrm{L}}-\widehat{\phi}_{\mathrm{L}})\right] \\
& + \left[K\cos(\widehat{\phi}_{\mathrm{R}}-\widehat{\phi}_{\mathrm{L}}) + L\sin(\widehat{\phi}_{\mathrm{R}}-\widehat{\phi}_{\mathrm{L}})\right] \\
& \quad \times \left[A_{\mathrm{R}}A_{\mathrm{L}}\left(\cos(\phi_{\mathrm{R}}-\widehat{\phi}_{\mathrm{R}})\sin(\phi_{\mathrm{L}}-\widehat{\phi}_{\mathrm{L}}) + \sin(\phi_{\mathrm{R}}-\widehat{\phi}_{\mathrm{R}})\cos(\phi_{\mathrm{L}}-\widehat{\phi}_{\mathrm{L}})\right)\right. \\
& \qquad \left. + A_{\mathrm{R}}\widehat{A}_{\mathrm{L}}\sin(\phi_{\mathrm{R}}-\widehat{\phi}_{\mathrm{R}}) + \widehat{A}_{\mathrm{R}}A_{\mathrm{L}}\sin(\phi_{\mathrm{L}}-\widehat{\phi}_{\mathrm{L}})\right]
\end{aligned}
\tag{B.3}
$$

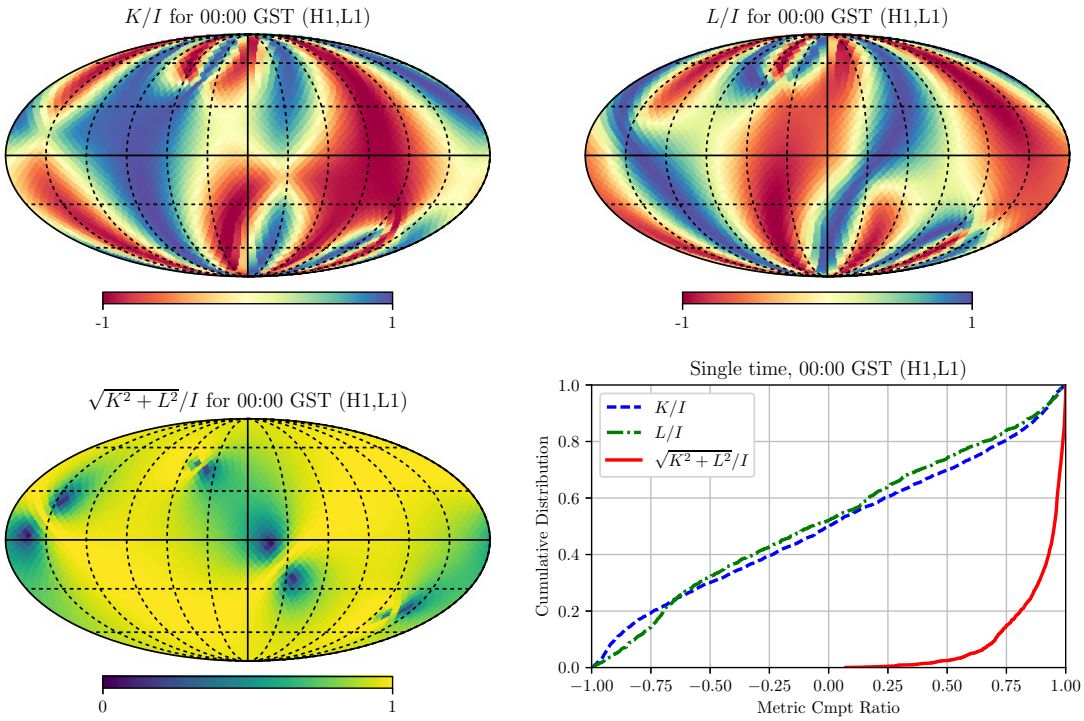

Figure A5. Plots of the metric element ratios K/I, L/I, and $\sqrt{K^2+L^2}/I$ versus sky position of targeted source, along with cumulative probability distributions of these ratios, assuming a randomly chosen sky location, for a brief observation at Greenwich sidereal time 00:00.

The likelihood ratio can be expanded, to first order, as

$$e^{\Lambda(\{\mathcal{A}^\mu\};x)} = e^{\Lambda_{\rm R}(A_{\rm R},\phi_{\rm R};\widehat{A}_{\rm R},\widehat{\phi}_{\rm R})+\Lambda_{\rm L}(A_{\rm L},\phi_{\rm L};\widehat{A}_{\rm L},\widehat{\phi}_{\rm L})+\Lambda_1(\mathcal{A};\widehat{\mathcal{A}})} \approx e^{\Lambda_{\rm R}(A_{\rm R},\phi_{\rm R};\widehat{A}_{\rm R},\widehat{\phi}_{\rm R})} e^{\Lambda_{\rm L}(A_{\rm L},\phi_{\rm L};\widehat{A}_{\rm L},\widehat{\phi}_{\rm L})} \left(1+\Lambda_1(\mathcal{A};\widehat{\mathcal{A}})\right) \tag{B.4}$$

In this form, we can factor the integrals in each of the terms; they all reduce to one of three forms:

$$\int_0^{2\pi}\int_0^{\infty} e^{-\frac{I}{2}A^2+IA\widehat{A}\cos(\phi-\widehat{\phi})}\frac{dA\,d\phi}{\sqrt{A}} = 2\pi\int_0^{\infty} e^{-\frac{I}{2}A^2} I_0(IA\widehat{A})\frac{dA}{\sqrt{A}} \tag{B.5a}$$

$$\int_0^{2\pi}\int_0^{\infty} e^{-\frac{I}{2}A^2+IA\widehat{A}\cos(\phi-\widehat{\phi})}\cos(\phi-\widehat{\phi})\sqrt{A}\,dA\,d\phi = 2\pi\int_0^{\infty} e^{-\frac{I}{2}A^2} I_1(IA\widehat{A})\sqrt{A}\,dA \tag{B.5b}$$

$$\int_0^{2\pi}\int_0^{\infty} e^{-\frac{I}{2}A^2+IA\widehat{A}\cos(\phi-\widehat{\phi})}\sin(\phi-\widehat{\phi})\sqrt{A}\,dA\,d\phi = 0 \tag{B.5c}$$

where $I_n(x) = i^{-n}J_n(ix)$ is the modified Bessel function, and we have used the Jacobi-Anger expansion[4], which tells us that

$$e^{IA\widehat{A}\cos(\phi-\widehat{\phi})} = I_0(IA\widehat{A}) + 2\sum_{n=1}^{\infty} I_n(IA\widehat{A})\cos(n[\phi-\widehat{\phi}]) \ . \tag{B.6}$$

Both of the remaining integrals can be done using equation (11.4.28) of [4], which says, in terms of the modified Bessel function, that, when $\mathrm{Re}(\nu+\mu)>0$ and $\mathrm{Re}(a^2)>0$,

$$\int_0^\infty e^{-a^2t^2}\, t^{\mu-1} I_\nu(bt)\, dt = \frac{\Gamma\left(\frac{\nu+\mu}{2}\right)\left(\frac{b}{2a}\right)^\nu}{2a^\mu\Gamma(\nu+1)}\ {}_1F_1\left(\frac{\nu+\mu}{2}, \nu+1, \frac{b^2}{4a^2}\right) \tag{B.7}$$

where ${}_1F_1(a,b,z) = M(a,b,z)$ is the confluent hypergeometric function. We apply this with $a^2 = I/2$, $b = I\widehat{A}$, $\mu = 1/2$ and $3/2$, and $\nu = 0$ and 1, respectively, in (B.5a) and (B.5b), to get

$$\int_0^{2\pi}\int_0^\infty e^{-\frac{I}{2}A^2 + IA\widehat{A}\cos(\phi-\widehat{\phi})}\frac{dA\, d\phi}{\sqrt{A}} = 2\pi\frac{\Gamma\left(\frac{1}{4}\right)}{2^{3/4}I^{1/4}}\ {}_1F_1\left(\frac{1}{4}, 1, \frac{I\widehat{A}^2}{2}\right) \tag{B.8a}$$

$$\int_0^{2\pi}\int_0^\infty e^{-\frac{I}{2}A^2 + IA\widehat{A}\cos(\phi-\widehat{\phi})}\cos(\phi-\widehat{\phi})\sqrt{A}\, dA\, d\phi = 2\pi\frac{\Gamma\left(\frac{5}{4}\right)\widehat{A}}{2^{3/4}I^{1/4}}\ {}_1F_1\left(\frac{5}{4}, 2, \frac{I\widehat{A}^2}{2}\right) \tag{B.8b}$$

We can use these to evaluate the integral for the $\mathcal{B}$-statistic (2.23) as

$$\begin{aligned}\mathcal{B}(x) \approx \frac{A}{8\pi^2}&\left(2\pi\frac{\Gamma\left(\frac{1}{4}\right)}{2^{3/4}I^{1/4}}\right)\left(2\pi\frac{\Gamma\left(\frac{1}{4}\right)}{2^{3/4}J^{1/4}}\right){}_1F_1\left(\frac{1}{4}, 1, \frac{I\widehat{A}_{\mathrm{R}}^2}{2}\right){}_1F_1\left(\frac{1}{4}, 1, \frac{J\widehat{A}_{\mathrm{L}}^2}{2}\right)\\ &\times\left\{1 + \left[K\sin(\widehat{\phi}_{\mathrm{R}}-\widehat{\phi}_{\mathrm{L}}) + L\cos(\widehat{\phi}_{\mathrm{R}}-\widehat{\phi}_{\mathrm{L}})\right]\widehat{A}_{\mathrm{R}}\widehat{A}_{\mathrm{L}}\right.\\ \times\left[\frac{1}{4}\left(\frac{{}_1F_1\left(\frac{5}{4},2,\frac{I\widehat{A}_{\mathrm{R}}^2}{2}\right)}{{}_1F_1\left(\frac{1}{4},1,\frac{I\widehat{A}_{\mathrm{R}}^2}{2}\right)}\right) + \frac{1}{4}\left(\frac{{}_1F_1\left(\frac{5}{4},2,\frac{J\widehat{A}_{\mathrm{L}}^2}{2}\right)}{{}_1F_1\left(\frac{1}{4},1,\frac{J\widehat{A}_{\mathrm{L}}^2}{2}\right)}\right) - \frac{1}{16}\left(\frac{{}_1F_1\left(\frac{5}{4},2,\frac{I\widehat{A}_{\mathrm{R}}^2}{2}\right)}{{}_1F_1\left(\frac{1}{4},1,\frac{I\widehat{A}_{\mathrm{R}}^2}{2}\right)}\right)\left(\frac{{}_1F_1\left(\frac{5}{4},2,\frac{J\widehat{A}_{\mathrm{L}}^2}{2}\right)}{{}_1F_1\left(\frac{1}{4},1,\frac{J\widehat{A}_{\mathrm{L}}^2}{2}\right)}\right)\right]\right\}\end{aligned} \tag{B.9}$$

Appendix C. Recovery of $\mathcal{F}$-Statistic

Our method expands the $\mathcal{B}$-statistic to first order in the metric components K and L. It has been shown in [2] that the Bayes factor constructed with a prior uniform in the $\{\mathcal{A}^{\check{\mu}}\}$ is equivalent to the $\mathcal{F}$-statistic, which we note in (2.20) has only zeroth- and first-order terms in these quantities. This means that applying the Taylor-expansion method with this prior should reproduce the *exact* $\mathcal{F}$-statistic.

If we replace the isotropic prior (2.22) with a uniform prior $\mathrm{pdf}(\mathcal{A}^{\check{1}}, \mathcal{A}^{\check{2}}, \mathcal{A}^{\check{3}}, \mathcal{A}^{\check{4}}|\mathcal{H}_f) = C$, the $\mathcal{B}$-statistic integral (2.23) becomes

$$\begin{aligned}\mathcal{B}(x) &= C\int_{-\infty}^{\infty}\int_{-\infty}^{\infty}\int_{-\infty}^{\infty}\int_{-\infty}^{\infty} e^{\Lambda(\{\mathcal{A}^{\check{\mu}}\};x)}\, d\mathcal{A}^{\check{1}}\, d\mathcal{A}^{\check{2}}\, d\mathcal{A}^{\check{3}}\, d\mathcal{A}^{\check{4}}\\ &= C\int_0^{2\pi}\int_0^{2\pi}\int_0^{\infty}\int_0^{\infty} e^{\Lambda(\{\mathcal{A}^{\check{\mu}}\};x)} A_{\mathrm{R}}A_{\mathrm{L}}\, dA_{\mathrm{R}}\, dA_{\mathrm{L}}\, d\phi_{\mathrm{R}}\, d\phi_{\mathrm{L}}\end{aligned} \tag{C.1}$$

The Taylor expansion of the likelihood, and the angular integrals, proceed as in Appendix B, and the only difference is that the two principal integrals (B.5a) and (B.5b), become

$$\int_0^{2\pi}\int_0^{\infty} e^{-\frac{I}{2}A^2+IA\widehat{A}\cos(\phi-\widehat{\phi})}\,A\,dA\,d\phi = 2\pi\int_0^{\infty} e^{-\frac{I}{2}A^2} I_0(IA\widehat{A})\,A\,dA \tag{C.2a}$$

$$\int_0^{2\pi}\int_0^{\infty} e^{-\frac{I}{2}A^2+IA\widehat{A}\cos(\phi-\widehat{\phi})}\cos(\phi-\widehat{\phi})\,A^2\,dA\,d\phi = 2\pi\int_0^{\infty} e^{-\frac{I}{2}A^2} I_1(IA\widehat{A})\,A^2\,dA \tag{C.2b}$$

Using (B.7) with $a^2 = I/2$, $b = I\widehat{A}$, $\mu = 2$ and 3, and $\nu = 0$ and 1, respectively, we find, in place of (B.8),

$$\int_0^{2\pi}\int_0^{\infty} e^{-\frac{I}{2}A^2+IA\widehat{A}\cos(\phi-\widehat{\phi})}\,A\,dA\,d\phi = \frac{2\pi}{I}\,{}_1F_1\left(1,1,\frac{I\widehat{A}^2}{2}\right) = \frac{2\pi}{I}e^{\frac{I\widehat{A}^2}{2}} \tag{C.3a}$$

$$\int_0^{2\pi}\int_0^{\infty} e^{-\frac{I}{2}A^2+IA\widehat{A}\cos(\phi-\widehat{\phi})}\cos(\phi-\widehat{\phi})\,A^2\,dA\,d\phi = \frac{2\pi\widehat{A}}{I}\,{}_1F_1\left(2,2,\frac{I\widehat{A}^2}{2}\right) = \frac{2\pi\widehat{A}}{I}e^{\frac{I\widehat{A}^2}{2}} \tag{C.3b}$$

where we have used (13.6.12) of [4], which states that ${}_1F_1(a,a,z) = e^z$. This then gives a statistic of

$$\mathcal{B}(x) \approx C\left(\frac{2\pi}{I}\right)\left(\frac{2\pi}{J}\right)e^{\frac{I\widehat{A}_{\mathrm{R}}^2+J\widehat{A}_{\mathrm{L}}^2}{2}}\left\{1+\left[K\sin(\widehat{\phi}_{\mathrm{R}}-\widehat{\phi}_{\mathrm{L}})+L\cos(\widehat{\phi}_{\mathrm{R}}-\widehat{\phi}_{\mathrm{L}})\right]\widehat{A}_{\mathrm{R}}\widehat{A}_{\mathrm{L}}(1+1-1)\right\} \tag{C.4}$$

So that, to first order in K and L,

$$\ln\frac{\mathcal{B}(x)}{\mathcal{B}(0)} \approx \frac{I\widehat{A}_{\mathrm{R}}^2}{2}+\frac{J\widehat{A}_{\mathrm{L}}^2}{2}+\left[K\sin(\widehat{\phi}_{\mathrm{R}}-\widehat{\phi}_{\mathrm{L}})+L\cos(\widehat{\phi}_{\mathrm{R}}-\widehat{\phi}_{\mathrm{L}})\right]\widehat{A}_{\mathrm{R}}\widehat{A}_{\mathrm{L}} \tag{C.5}$$

Which is indeed the form given in (2.20) for the exact $\mathcal{F}$-statistic.

Appendix D. Relationship to High-SNR Approximation

Recent work[10] by Dhurandhar, Krishnan and Willis (hereafter DKW) contains a different approximate expression for the $\mathcal{B}$-statistic, derived in the limit of high signal-to-noise ratio, but without assumptions on the form of the metric. In their notation, the approximate form is written [[10] equation (104)]

$$\mathcal{B}(x) \approx \left(\frac{\pi^2}{2(\zeta^2-k^2)}\right)\left[\frac{e^{\frac{1}{2}\widehat{\mathbf{B}}^\dagger\mathbf{N}\widehat{\mathbf{B}}}}{(|\widehat{\mathcal{B}}_1||\widehat{\mathcal{B}}_2|)^{\frac{3}{2}}}\right] \tag{D.1}$$

To make contact with our results, we collect here the conversion between DKW's notation and ours. Their metric elements are $\zeta = I = J$ (they limit attention to

the long-wavelength limit) and $\kappa = L + iK$, with $k = |\kappa| = \sqrt{K^2 + L^2}$. They define complex amplitudes

$$\mathcal{B}_1 = h_0 e^{-2i\phi_0} \frac{(1+\chi)^2}{4} e^{-2i\psi} = A_{\mathrm{R}} e^{-\frac{i}{2}(3\phi_{\mathrm{R}} + \phi_{\mathrm{L}})} = \mathcal{B}_4^* \tag{D.2a}$$

$$\mathcal{B}_2 = h_0 e^{-2i\phi_0} \frac{(1-\chi)^2}{4} e^{2i\psi} = A_{\mathrm{L}} e^{-\frac{i}{2}(\phi_{\mathrm{R}} + 3\phi_{\mathrm{L}})} = \mathcal{B}_3^* \tag{D.2b}$$

and a complex metric

$$\mathbf{N} \equiv \{N_{\mu\nu}\} = \frac{1}{2} \begin{pmatrix} \zeta & \kappa^* & 0 & 0 \\ \kappa & \zeta & 0 & 0 \\ 0 & 0 & \zeta & \kappa^* \\ 0 & 0 & \kappa & \zeta \end{pmatrix} \tag{D.3}$$

from which we see

$$\begin{aligned} \frac{1}{2}\widehat{\mathbf{B}}^\dagger \mathbf{N} \widehat{\mathbf{B}} &= \mathrm{Re}\left(\widehat{A}_{\mathrm{R}} e^{\frac{i}{2}(3\widehat{\phi}_{\mathrm{R}} + \widehat{\phi}_{\mathrm{L}})} [L - iK] \widehat{A}_{\mathrm{L}} e^{-\frac{i}{2}(\widehat{\phi}_{\mathrm{R}} + 3\widehat{\phi}_{\mathrm{L}})} \right) \\ &= \frac{1}{2} I \widehat{A}_{\mathrm{R}}^2 + \frac{1}{2} J \widehat{A}_{\mathrm{L}}^2 + \widehat{A}_{\mathrm{R}} \widehat{A}_{\mathrm{L}} \left[K \sin(\widehat{\phi}_{\mathrm{R}} - \widehat{\phi}_{\mathrm{L}}) + L \cos(\widehat{\phi}_{\mathrm{R}} - \widehat{\phi}_{\mathrm{L}}) \right] = \mathcal{F} \end{aligned} \tag{D.4}$$

and therefore their approximation can be written

$$\mathcal{B}(x) \approx \left(\frac{\pi^2}{2(IJ - K^2 - L^2)} \right) \left[\frac{e^{\mathcal{F}}}{(\widehat{A}_{\mathrm{R}} \widehat{A}_{\mathrm{L}})^{\frac{3}{2}}} \right] \tag{D.5}$$

Written in this form, we see that the result is the same as equation (5.37) of [3]. The difference between this and (3.4) is the normalization constant. (Note that DKW use an improper prior equivalent to $A = 2\pi^2$.)

References

[1] Jaranowski P, Królak A and Schutz B F 1998 *Phys. Rev. D.* **58** 063001 (*Preprint* `gr-qc/9804014`)

[2] Prix R and Krishnan B 2009 *Class. Quant. Grav.* **26** 204013 (*Preprint* `arXiv:0907.2569`)

[3] Whelan J T, Prix R, Cutler C J and Willis J L 2014 *Class. Quant. Grav.* **31** 065002 (*Preprint* `1311.0065`)

[4] Abramowitz M and Stegun I A 1964 *Handbook of Mathematical Functions* (National Bureau of Standards)

[5] Dergachev V 2012 *Phys. Rev. D.* **85** 062003 (*Preprint* `1110.3297`)

[6] Searle A C 2008 *ArXiv E-Prints* (*Preprint* `0804.1161`)

[7] Jones E, Oliphant T, Peterson P *et al.* 2001– SciPy: Open source scientific tools for Python [Online; accessed 2018 Oct 1] URL `http://www.scipy.org/`

[8] Collaboration T L S and the Virgo Collaboration LSC Algorithm Library software suite URL `https://wiki.ligo.org/Computing/DASWG/LALSuite`

[9] Vallisneri M, Kanner J, Williams R, Weinstein A and Stephens B 2015 *Journal of Physics: Conference Series* **610** 012021 (*Preprint* `arXiv:1410.4839`)

[10] Dhurandhar S, Krishnan B and Willis J L 2017 (*Preprint* `1707.08163`)